

A Two-time-level Model for Mission and Flight Planning of an Inhomogeneous Fleet of Unmanned Aerial Vehicles

Johannes Schmidt
Armin Fügenschuh

A Two-time-level Model for Mission and Flight Planning of an Inhomogeneous Fleet of Unmanned Aerial Vehicles

Johannes Schmidt ^{a*} Armin Fügenschuh ^a

March 18, 2021

Abstract

We consider the mission and flight planning problem for an inhomogeneous fleet of unmanned aerial vehicles (UAVs). Therein, the mission planning problem of assigning targets to a fleet of UAVs and the flight planning problem of finding optimal flight trajectories between a given set of waypoints are combined into one model and solved simultaneously. Thus, trajectories of an inhomogeneous fleet of UAVs have to be specified such that the sum of waypoint-related scores is maximized, considering technical and environmental constraints. Several aspects of an existing basic model are expanded to achieve a more detailed solution. A two-level time grid approach is presented to smooth the computed trajectories. The three-dimensional mission area can contain convex-shaped restricted airspaces and convex subareas where wind affects the flight trajectories. Furthermore, the flight dynamics are related to the mass change, due to fuel consumption, and the operating range of every UAV is altitude-dependent. A class of benchmark instances for collision avoidance is adapted and expanded to fit our model and we prove an upper bound on its objective value. Finally, the presented features and results are tested and discussed on several test instances using GUROBI as a state-of-the-art numerical solver.

Keywords: Mixed-Integer Nonlinear Programming, Mission Planning, Inhomogeneous Fleet, Time Windows, Linearization Methods

1 Introduction

Due to their variety and flexibility, unmanned aerial vehicles (UAVs) have many possible applications. Next to the long-studied military use [5], also many companies make efforts to incorporate them into their processes, e.g., in parcel delivery [24], but for an efficient and autonomous use, it is crucial to plan the considered task carefully since not only the technical parameters of the used UAV but also the weather and maybe other airborne UAVs must be taken into account. Furthermore, the mission area can contain airports, power plants, or mountains, restricting the airspace and the possible routes. Incorporating all these conditions into the planning process can make the resulting problem very intricate to solve.

The flight planning problem for a given number of inhomogeneous UAVs asks to calculate a flight trajectory between a set of given waypoints for any considered UAV, complying with its technical parameters and the related flight dynamics. The mission planning problem for an inhomogeneous fleet of UAVs is a version of the well-studied Vehicle Routing Problem (VRP). Therein, a fleet of vehicles is assigned to a set of waypoints while the

^aBrandenburg University of Technology Cottbus-Senftenberg,
Platz der Deutschen Einheit 1, 03046 Cottbus, Germany,
{johannes.schmidt,fuegenschuh}@b-tu.de

*Corresponding author

overall path should have minimal length. Next to the classical VRP, several of its variants are incorporating additional constraints, e.g., time windows or backhauls. Further information about this problem class can be found in [27].

We consider the mission and flight planning problem for an inhomogeneous fleet of UAVs as a variant of the VRP with time windows, where further constraints regarding the flight dynamics of the considered UAVs and the environment have to be taken into account. UAVs do not rely on streets and can navigate through the air almost freely with some related conditions like minimum velocity, maximum altitude, or restricted airspaces. Furthermore, safety distances in aviation are stricter than in road traffic, where they are negligible for modeling. Wind affects the flight of every UAV since their movement is always relative to the surrounding atmosphere. Next to environmental parameters, the mass of a flying object has a strong influence on its flight dynamics. Several characteristics, e.g., maximum acceleration, maximum reachable altitude, or fuel consumption, depend on it [23]. Finally, the operating range has to be observed if the connection of a UAV and its ground control station is not a satellite link, but a UHF/VHF connection instead.

In the literature, the mission planning problem for UAVs applies to a large number of practical tasks, e.g., military operations [16], the observation of icebergs [1], or the reconstruction of terrain from two-dimensional data [26], but often, the calculation of the related flight trajectories is simplified or neglected.

An extensive survey on the evolving field of civil applications for UAVs and possible optimization approaches can be found in [19]. Due to the great interest in the autonomous use of UAVs and the large number of related optimization approaches, we only highlight some recent publications, where mission and flight planning is considered. Ramirez *et al.* [20] use a genetic algorithm to assign several tasks to a fleet of inhomogeneous UAVs considering technical parameters of the different types of UAVs, restricted airspaces, and time windows. Zhen, Xing, and Gao [29] combine an ant colony algorithm for assigning missions to a set of homogeneous UAVs with a Dubins curve to generate the trajectory of every UAV. The resulting paths are affected by technical parameters of the considered UAV, collision avoidance constraints, and restricted airspaces. Ribeiro *et al.* [22] use a mixed-integer linear program (MILP) to organize the observation of conveyor belts in a mining site. Their approach is rather combinatorial without exact trajectories but incorporates energy consumption and the possibility to place and use charging stations. Li *et al.* [17] apply an ant colony algorithm combined with the metropolis criterion to the problem of finding optimal trajectories for a fleet of homogeneous UAVs on a grid map, regarding a given safety distance between the UAVs and given obstacles. Glock and Meyer [10] present a neighborhood search algorithm to assign possible sampling locations after fire or chemical incidents to a set of UAVs and plan their trajectories to maximize the collected information in a given time horizon. Flight dynamics, i.e., maximum velocity, acceleration, and battery level of the homogeneous fleet, are translated into travel times between target locations. Coutinho, Fliege, and Battarra [6] formulate the problem of surveying a set of locations in the aftermath of a disaster by pilotless gliders as a mixed-integer nonlinear problem (MINLP). By applying several linearization techniques, they achieve an MILP computing trajectories for several aircrafts from a starting point to a set of possible landing areas within an obstacle-free airspace assuming constant weather conditions. Cheng, Adulyasak, and Rousseau [4] derive a branch-and-cut algorithm to solve an MINLP describing the problem of multi-trip parcel delivery by a homogeneous fleet of UAVs. Considering constant altitude and velocity, their energy consumption is modeled using a mass-dependent, nonlinear function, and trajectories are given by distances and travel times. Thibbotuwawa *et al.* [25] set up an MILP to plan the supply of a set of customers with an inhomogeneous fleet of UAVs under weather uncertainty. Their proposed model incorporates several weather zones, each with related wind con-

ditions, energy consumption, and collision avoidance. In terms of the flight dynamics, it lacks the exact trajectory, only computing the sequence of visited customers. Kai *et al.* [14] give an MILP to plan the trajectory of a UAV visiting a given set of waypoints taking into account detailed flight dynamics. In terms of environmental constraints, the therein presented model lacks weather conditions and restricted airspaces. Xia, Wang, and Wang [28] formulate the problem of controlling moving ships in emission control areas by UAVs, stationed at the coast, as an MILP and compare it with a Lagrangian relaxation. The UAVs are assigned to computed waypoints, where they meet a vessel. Though, besides the battery level, no flight dynamics are taken into account. Albert, Leira, and Imsland [1] present an integer linear optimization model for the observation of drifting icebergs in arctic areas to support shipping using a homogeneous fleet of UAVs deployed at a ship. Their approach uses Dubins curves to compute trajectories and can update the present path during the mission by a new run of the optimization model. But therefore, it neglects most of the flight dynamics to speed up the solution process. Chen *et al.* [3] consider a UAV as particle affected by different force fields and plan trajectories avoiding given obstacles. The resulting problem is solved using optimal control theory but neglects flight dynamics and weather conditions.

Within the flight planning process, collision avoidance and conflict resolution is a crucial field to ensure the safe operation of aircrafts and avoid significant harm. It considers a given number of aircraft within the same airspace and asks for the best control changes for each of them to achieve collision-free trajectories. If the problem is stated in three dimensions, also altitude changes are possible to resolve conflicts. Although the process of solving potential conflicts between midair aircraft is automated [15], considering this aspect already in the operation planning phase can reduce the number of conflicts and errors later.

An extensive review about the field of conflict detection and resolution and related solution methods can be found in [21]. Due to its currency, we further mention only two forthcoming approaches. Dias, Rahme, and Rey [7] derive a two-stage algorithm for conflict resolution using a mixed-integer quadratic and mixed-integer linear problem. It computes collision-free linear trajectories for all aircrafts, while every aircraft reaches its initial end position. Their model is tested on the class of benchmark instances that we also adapt for our model. In [12], Hoch *et al.* consider collision avoidance as a non-stop disjoint trajectory problem, where commodities are shipped through a time-expanded graph without coming across each other. They study the general properties of this problem and examine different graph classes which can be applied as takeoff/landing phase with several aircraft or airspaces with a fixed number of airports and aircraft. Due to the underlying network, this approach lacks detailed flight trajectories.

We contribute to the state-of-the-art by considering the mission and flight planning problem for an inhomogeneous fleet of UAVs in a mixed-integer non-linear programming framework, including detailed flight dynamics of the different UAVs, the effect of wind in different subareas and altitudes, convex shaped restricted airspaces, and collision avoidance. Furthermore, we extend several of its aspects to enhance the quality of the computed solution. The novelty of our approach is the combination of assigning waypoints to the participating UAVs and calculating detailed flight trajectories at the same time. This paper extends the work presented in [9]. The newly incorporated aspects are the following: By the combination of two different time discretizations, the computed flight trajectories have an increased level of detail. We incorporate mass-dependent maximum velocity, maximum acceleration, maximum reachable altitude, and a mass-dependent fuel consumption into the presented model. The operating range of every UAV is defined dependent on altitude, assuming no sky propagation, and the height of the used antenna. Restricted airspaces are generalized to convex shaped areas and wind affects any UAV within spec-

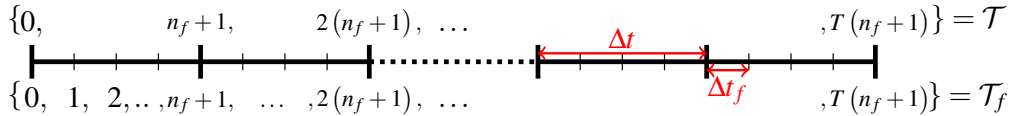


Figure 1: Sets and time step lengths for the layers \mathcal{T} and \mathcal{T}_f of the two-level time grid approach.

ified convex subareas. Considering collision avoidance, we adapt and extend a class of benchmark problems to fit our model and derive upper bounds for their necessary amount of discrete time steps in the two- and three-dimensional case.

This paper is structured as follows. In section 2, the basic model is set up by applying the two-level time discretization. Furthermore, the computation of the UAVs flight dynamics, the operating range, the restricted airspaces, and the influence of wind are expanded to allow more realistic constraints and achieve high-quality solutions. In section 3, a class of benchmark instances for collision avoidance is adapted to the introduced model and upper bounds for the necessary time horizon are given. The effect of the derived modifications and results is tested in several scenarios in section 4, including the influence of the time discretization on the computation time, comparison between the derived upper bounds and the computed optimal solution for collision avoidance problems, and a detailed discussion of particular aspects of our model. We summarize the presented results and give directions for future work in section 5.

2 Two-level Time Model

If the velocity and the acceleration can change only at any discrete time step, the step length has to decrease to smoothen the computed trajectories. Thus, more time steps are necessary to cover the same time interval, leading to more complex instances and slower solution processes. In the following, we present a possibility to achieve smooth trajectories by using two different, coupled time discretizations and apply it to the model in [9]. Afterwards, the derived two-level time discretization model is extended in several ways. A list of all used sets can be found in table 1. The parameters and variables within the two-level time discretization model are given in tables 2 and 3, while the additional parameters and variables of the complete extended model are described in tables 4 and 5.

The time horizon $[0, \Delta t T]$, for a given number of time steps T and time step length Δt , is discretized in two different ways to achieve a better discretization without an increase in the number of time steps and discrete decision variables. Let n_f denote the number of fine time steps between two adjacent time steps in \mathcal{T} . For the first discretization, the step size Δt is applied, but the set \mathcal{T} contains all multiples of $n_f + 1$ in the interval $[0, (n_f + 1)T]$, i.e., $\mathcal{T} = \{0, n_f + 1, \dots, (n_f + 1)T\}$. This discretization is applied to the binary variables to model the possible decisions. Second, each time step $t \in \{0, 1, \dots, T\}$ is divided into n_f (fine) time steps, resulting in a step size $\Delta t_f = \frac{\Delta t}{n_f + 1}$ and a set $\mathcal{T}_f = \{0, 1, \dots, (n_f + 1)T\}$. This fine time approximation is applied to all continuous variables to refine the computed trajectories. Furthermore, a function $\llbracket t \rrbracket : \mathcal{T}_f \rightarrow \mathcal{T}$ of the form

$$\llbracket t \rrbracket = \left\lfloor \frac{t}{n_f + 1} \right\rfloor (n_f + 1) \quad (1)$$

is necessary to map the fine time steps to their coarse counterpart, always rounding down. As abbreviations $\mathcal{T}^- = \mathcal{T} \setminus \{(n_f + 1)T\}$ and $\mathcal{T}_f^- = \mathcal{T}_f \setminus \{(n_f + 1)T\}$ are used. Figure 1 holds an illustration of this two-level time grid approach. Using the two-level time grid approach, the mission and flight planning problem for an inhomogeneous fleet of UAVs is

Table 1: Overview of the sets used in the extended mission and flight planning model.

Symbol	Index	Definition
\mathcal{L}_u	i	set of altitude bands of UAV u
$\mathcal{L}_{0,u} = \mathcal{L}_u \cup \{0\}$	i	set of altitude bands of UAV u including the ground
\mathcal{P}	p	set of all wind zones
\mathcal{Q}	q	set of all restricted airspaces
$\mathcal{T} = \{0, n_f + 1, \dots, (n_f + 1)T\}$	t	set of discrete time steps
$\mathcal{T}^- = \{0, n_f + 1, \dots, (n_f + 1)T - 1\}$	t	set of discrete time steps excluding the last one
$\mathcal{T}_f = \{0, 1, \dots, (n_f + 1)T\}$	t	set of refined discrete time steps
$\mathcal{T}_f^- = \{0, 1, \dots, (n_f + 1)T - 1\}$	t	set of refined discrete time steps excluding the last one
$\mathcal{T}_w \subseteq \mathcal{T}$	t	set of time steps at which waypoint w can be visited
\mathcal{U}	u	set of all considered UAVs
\mathcal{V}_u	j	set of throttle bands of UAV u
\mathcal{W}	w	set of all waypoints to be visited

given by

$$\vec{r}_u(0) = \vec{R}_u^0 \quad \forall u \in \mathcal{U}, \quad (2.1)$$

$$\vec{r}_u((n_f + 1)T) = \vec{R}_u^T \quad \forall u \in \mathcal{U}, \quad (2.2)$$

$$\|\vec{r}_u(t) - \vec{G}_u\|_2 \leq \varrho_u \quad \forall u \in \mathcal{U}, t \in \mathcal{T}_f, \quad (2.3)$$

$$\underline{h}_u b_u(\lfloor t \rfloor) \leq r_u^z(t) \leq \bar{h}_u b_u(\lfloor t \rfloor) \quad \forall u \in \mathcal{U}, t \in \mathcal{T}_f, \quad (2.4)$$

$$r_u^i(t + 1) = r_u^i(t) + \Delta t_f v_u^i(t) + \Delta t_f w^i(\lfloor t \rfloor) b_u(\lfloor t \rfloor) + \frac{(\Delta t_f)^2}{2} a_u^i(t) \quad \forall u \in \mathcal{U}, t \in \mathcal{T}_f^-, i \in \{x, y\}, \quad (2.5)$$

$$v_u^i(t + 1) = v_u^i(t) + \Delta t_f a_u^i(t) \quad \forall u \in \mathcal{U}, t \in \mathcal{T}_f^-, i \in \{x, y\}, \quad (2.6)$$

$$r_u^z(t + 1) = r_u^z(t) + \Delta t_f (v_u^{z,+}(t) - v_u^{z,-}(t)) \quad \forall u \in \mathcal{U}, t \in \mathcal{T}_f, \quad (2.7)$$

$$\underline{v}_u(t) b_u(\lfloor t \rfloor) \leq \|\vec{v}_u(t)\|_2 \leq \bar{v}_u(t) b_u(\lfloor t \rfloor) \quad \forall u \in \mathcal{U}, t \in \mathcal{T}_f, \quad (2.8)$$

$$\bar{a}_u(t) b_u(\lfloor t \rfloor) \geq \|\vec{a}_u(t)\|_2 \quad \forall u \in \mathcal{U}, t \in \mathcal{T}_f, \quad (2.9)$$

Table 2: Overview of the parameters used in the mission and flight planning model of section 2.

Symbol	Domain	Definition
\bar{a}_u	\mathbb{R}_+	maximum acceleration of UAV u
$\bar{c}_q(t)$	\mathbb{R}^3	location of the top-right corner of restricted airspace q at time step t
$\bar{c}_q(t)$	\mathbb{R}^3	location of the bottom-left corner of restricted airspace q at time step t
F_u	\mathbb{R}_+	maximum fuel of UAV u
\vec{G}_u	\mathbb{R}^3	location of the ground control station for UAV u
$H_{u,i}$	\mathbb{R}_+	altitude limit of UAV u in altitude band i
\bar{h}_u	\mathbb{R}_+	maximum flight altitude of UAV u
\underline{h}_u	$[0, \bar{h}_u]$	minimum flight altitude of UAV u
M^i	\mathbb{R}_+	sufficiently large constants with different magnitude for $i \in \{dist, air, fuel, alt, vel\}$
n_f	$\mathbb{N} \cup \{0\}$	number of fine time steps
\vec{p}_w	\mathbb{R}^3	location of waypoint w
\vec{R}_u^0	\mathbb{R}^3	start location of UAV u
\vec{R}_u^T	\mathbb{R}^3	end location of UAV u
S_w	\mathbb{R}_+	score value for visiting waypoint w
$\bar{v}_u^{z,+}$	\mathbb{R}_+	maximum climb rate of UAV u
$\bar{v}_u^{z,-}$	\mathbb{R}_+	maximum descent rate of UAV u
\bar{v}_u	\mathbb{R}_+	maximum velocity of UAV u
\underline{v}_u	$[0, \bar{v}_u]$	minimum velocity of UAV u
$\vec{w}(t)$	\mathbb{R}^2	horizontal wind velocity at time step t
T	\mathbb{N}	number of coarse discrete time steps
Δt	\mathbb{R}_+	length of one discrete time step
Δt_f	\mathbb{R}_+	length of one refined discrete time step
$\delta_{u,w}$	$[0, \varrho_u]$	maximum operational distance of UAV u to waypoint w
$\bar{\varepsilon}$	\mathbb{R}_+^3	required minimum safety distance between two UAVs
$\eta_{u,i,j}$	\mathbb{R}_+	fuel consumption of UAV u in altitude band i and throttle band j
$\theta_{u,j}$	\mathbb{R}_+	velocity limit of UAV u in throttle band j
$\llbracket t \rrbracket$	\mathcal{T}	fine-to-coarse mapping for time discretization
ξ_u	\mathbb{R}_+	fuel surplus of UAV u for climbing
ϱ_u	\mathbb{R}_+	maximum operating range of UAV u

Table 3: Overview of the variables used in the mission and flight planning model of section 2.

Symbol	Domain	Definition
$\vec{a}_u(t)$	\mathbb{R}^2	variable indicating the acceleration of UAV u at time step t in horizontal direction
$b_u(t)$	$\{0, 1\}$	binary variable indicating whether UAV u is airborne at time step t
$b_u^+(t)$	$\{0, 1\}$	binary variable indicating whether the task of UAV u started at time step t or before
$b_u^-(t)$	$\{0, 1\}$	binary variable indicating whether UAV u is still on its way at time step t
$d_{u,w}(t)$	$\{0, 1\}$	binary variable indicating whether UAV u visits waypoint w at time step t
$\vec{e}_{u,u'}(t)$	$\{0, 1\}^3$	binary variable indicating whether the distance between UAVs u, u' is smaller than the safety distance in top-right direction
$\underline{\vec{e}}_{u,u'}(t)$	$\{0, 1\}^3$	binary variable indicating whether the distance between UAVs u, u' is smaller than the safety distance in bottom-left direction
$\vec{f}_{u,q}(t)$	$\{0, 1\}^3$	binary variable indicating whether UAV u is below-left the top-right corner of the restricted airspace q at time step t
$\underline{\vec{f}}_{u,q}(t)$	$\{0, 1\}^3$	binary variable indicating whether UAV u is upper-right the bottom-left corner of the restricted airspace q at time step t
$g_u(t)$	\mathbb{R}_+	variable indicating the amount of remaining fuel of UAV u at time step t
$\vec{r}_u(t)$	\mathbb{R}^3	variable indicating the position of UAV u at time step t
$s_{u,i,j}(t)$	$\{0, 1\}$	binary variable indicating whether UAV u is in altitude band i and throttle band j at time step t
$\vec{v}_u(t)$	\mathbb{R}^2	variable indicating the horizontal velocity of UAV u at time step t
$v_u^{z,+}(t)$	$\left[0, \bar{v}_u^{z,+}\right]$	variable indicating the climb rate of UAV u at time step t
$v_u^{z,-}(t)$	$\left[0, \bar{v}_u^{z,-}\right]$	variable indicating the descent rate of UAV u at time step t

Table 4: Overview of the additional parameters introduced in sections 2.1 - 2.5.

Symbol	Domain	Definition
A_u	\mathbb{R}_+	height of the antenna at the ground control station of UAV u
C	\mathbb{R}_+	sufficiently large constant
$\vec{c}_{q,i}(t)$	\mathbb{R}^3	normal vector of hyperplane i of restricted airspace q at time step t
$c_{q,i}^{rhs}(t)$	\mathbb{R}	right-hand side of the coordinate form related to hyperplane i of restricted airspace q at time step t
E	\mathbb{R}_+	radius of the earth
m_u	\mathbb{R}_+	empty weight of UAV u
N_p^P	\mathbb{N}	number of hyperplanes describing wind zone p
N_q^Q	\mathbb{N}	number of hyperplanes describing restricted airspace q
$\vec{n}_{p,i}(t)$	\mathbb{R}^3	normal vector of hyperplane i of wind zone p at time step t
$n_{p,i}^{rhs}(t)$	\mathbb{R}	right-hand side of the coordinate form related to hyperplane i of wind zone p at time step t
$\bar{v}_u^{z,+0}$	\mathbb{R}_+	maximum climb rate of UAV u at takeoff
$\bar{v}_{u,i,j}^{z,+}$	\mathbb{R}_+	maximum climb rate of UAV u in altitude band i and throttle band j
$\bar{v}_{u,i,j}^{z,-}$	\mathbb{R}_+	maximum descend rate of UAV u in altitude band i and throttle band j
$\bar{v}_{u,i}$	\mathbb{R}_+	maximum velocity of UAV u in altitude band i
$\vec{w}_{u,p,i}(t)$	\mathbb{R}^3	
$\vec{w}_l(t)$	\mathbb{R}^2	horizontal wind velocity in altitude band l at time step t
$\theta_{u,i,j}$	\mathbb{R}_+	velocity limit of UAV u in altitude band i and throttle band j
ϱ^{alt}	\mathbb{R}_+	change of operating range per unit of altitude
ϱ^{init}	\mathbb{R}_+	operating range on ground level
φ_u^{acc}	\mathbb{R}_-	obtainable percentage of the maximum velocity and acceleration per unit of fuel for UAV u
$\varphi_u^{alt,1}$	$[0, 1)$	proportion of initial fuel for which UAV u can reach its maximum altitude
$\varphi_u^{alt,2}$	$[0, 1)$	constant to set initial reachable altitude of UAV u
φ_u^{fuel}	\mathbb{R}	additional fuel consumption for every remainig unit of fuel of UAV u

Table 5: Overview of the additional variables introduced in sections 2.1 - 2.5.

Symbol	Domain	Definition
$\bar{b}_u(t)$	$\{0, 1\}$	binary variable indicating whether UAV u is airborne and has minimum velocity at time step t
$f_{u,q,i}(t)$	$\{0, 1\}$	binary variable indicating whether UAV u is inside restricted airspace q regarding hyperplane i at time step t
$w_{u,p,i}(t)$	$\{0, 1\}$	binary variable indicating whether UAV u is inside wind zone p regarding hyperplane i at time step t
$w_{u,p}(t)$	$\{0, 1\}$	binary variable indicating whether UAV u is inside wind zone p at time step t

$$b_u(t) = b_u^+(t) + b_u^-(t) - 1 \quad \forall u \in \mathcal{U}, t \in \mathcal{T}, \quad (2.10)$$

$$b_u^-(t+1) \leq b_u^-(t) \quad \forall u \in \mathcal{U}, t \in \mathcal{T}^-, \quad (2.11)$$

$$b_u^+(t) \leq b_u^+(t+1) \quad \forall u \in \mathcal{U}, t \in \mathcal{T}^-, \quad (2.12)$$

$$\|\vec{r}_u(t) - \vec{p}_w\|_3 \leq \delta_{u,w} + M^{dist}(1 - d_{u,w}(t)) \quad \forall u \in \mathcal{U}, w \in \mathcal{W}, t \in \mathcal{T}, \quad (2.13)$$

$$\sum_{u \in \mathcal{U}, t \in \mathcal{T}_w} d_{u,w}(t) \leq 1 \quad \forall w \in \mathcal{W}, \quad (2.14)$$

$$\vec{c}_q(\llbracket t \rrbracket) - M^{dist} \vec{f}_{u,q}(\llbracket t \rrbracket) \leq \vec{r}_u(t) \leq \vec{c}_q(\llbracket t \rrbracket) + M^{dist} \vec{f}_{u,q}(\llbracket t \rrbracket) \quad \forall u \in \mathcal{U}, q \in \mathcal{Q}, t \in \mathcal{T}_f, \quad (2.15)$$

$$\vec{1} \cdot \vec{f}_{u,q}(t) + \vec{1} \cdot \vec{f}_{u,q}(t) \leq 5 \quad \forall u \in \mathcal{U}, q \in \mathcal{Q}, t \in \mathcal{T}, \quad (2.16)$$

$$\vec{r}_{u'}(t) + \varepsilon - M^{dist} \vec{e}_{u,u'}(\llbracket t \rrbracket) \leq \vec{r}_u(t) \leq \vec{r}_{u'}(t) - \varepsilon + M^{dist} \vec{e}_{u,u'}(\llbracket t \rrbracket) \quad \forall u, u' \in \mathcal{U} : u < u', t \in \mathcal{T}_f, \quad (2.17)$$

$$\vec{1} \cdot \vec{e}_{u,u'}(t) + \vec{1} \cdot \vec{e}_{u,u'}(t) \leq 7 - b_u(t) - b_{u'}(t) \quad \forall u, u' \in \mathcal{U} : u < u', t \in \mathcal{T}, \quad (2.18)$$

$$g_u(0) = F_u \quad \forall u \in \mathcal{U}, \quad (2.19)$$

$$g_u(t+1) = g_u(t) - \Delta t_f \left(\xi_u v_u^{z,+} + \sum_{i \in \mathcal{L}_u, j \in \mathcal{V}_u} \eta_{u,i,j} s_{u,i,j}(\llbracket t \rrbracket) \right) \quad \forall u \in \mathcal{U}, t \in \mathcal{T}_f^-, \quad (2.20)$$

$$\sum_{i \in \mathcal{L}_u, j \in \mathcal{V}_u} s_{u,i,j}(t) = b_u(t) \quad \forall u \in \mathcal{U}, t \in \mathcal{T}, \quad (2.21)$$

$$\sum_{j \in \mathcal{V}_u} \theta_{u,j} \left(\sum_{i \in \mathcal{L}_u} s_{u,i,j}(\|t\|) \right) = \|\vec{v}_u(t)\|_2 \quad \forall u \in \mathcal{U}, t \in \mathcal{T}_f, \quad (2.22)$$

$$\sum_{i \in \mathcal{L}_u} H_{u,i-1} \left(\sum_{j \in \mathcal{V}_u} s_{u,i,j}(\|t\|) \right) \leq r_u^z(t) \leq \sum_{i \in \mathcal{L}_u} H_{u,i} \left(\sum_{j \in \mathcal{V}_u} s_{u,i,j}(\|t\|) \right) \quad \forall u \in \mathcal{U}, t \in \mathcal{T}_f. \quad (2.23)$$

with the objective function

$$\max \sum_{u \in \mathcal{U}, w \in \mathcal{W}, t \in \mathcal{T}} S_w d_{u,w}(t) - \frac{1}{|\mathcal{T}_f|} \sum_{u \in \mathcal{U}, t \in \mathcal{T}} \frac{t}{M^{air}} b_u(t) + \frac{1}{|\mathcal{T}_f|} \sum_{u \in \mathcal{U}, t \in \mathcal{T}_f} \left(\frac{g_u(t)}{M^{fuel}} + \frac{r_u^z(t)}{M^{alt}} - \frac{\|\vec{v}_u(t)\|_2}{M^{vel}} \right), \quad (3)$$

where $\|\cdot\|_2$ and $\|\cdot\|_3$ denote the two and three-dimensional Euclidean norm, respectively. Constraints (2.1) and (2.2) fix the respective start and end location of every UAV, while (2.3) limits their maximum operating range. The maximum and minimum altitude of the considered UAVs is restricted by (2.4). Equations (2.5) and (2.6) are a discretization of the Newton's equations of motion to compute the exact flight trajectory together with the altitude changes in (2.7). The UAVs velocity and acceleration is bounded by (2.8) and (2.9). In (2.10) – (2.12) it is ensured, that any UAV can only take off once and remain on the ground after landing. The visit of the given waypoints is managed by (2.13) and (2.14), guaranteeing that the respective UAV is inside the required operational range and every waypoint is only visited once. Constraints (2.15) and (2.16) let a UAV avoid the given restricted airspaces, while (2.17) and (2.18) manage the collision avoidance between any pair of UAVs. The correct computation of the UAVs fuel consumption is ensured by equations (2.19) – (2.23).

The presented model has to be linearized to achieve a mixed-integer linear problem. We do this according to the methods shown in [9].

2.1 Flight Dynamics

In the given model, the left part of equation (2.8) forces every UAV to fly with at least minimum velocity as soon as it takes off. If one of the deployed UAVs cannot accelerate to its minimum velocity within a single time step, it would have to stay on the ground and thus would not be used for mission planning. To overcome this drawback, we define a new binary variable $\bar{b}_u(t)$, indicating whether the minimum velocity has to hold.

Proposition 2.1. *Let $\bar{t}_u := (n_f + 1) \left\lceil \frac{v_u}{\bar{a}_u \Delta t} \right\rceil$ for UAV $u \in \mathcal{U}$. Then the equation*

$$\bar{b}_u(t) \geq \sum_{t'=t-\bar{t}_u}^{t+\bar{t}_u} b_u(t') - 2\bar{t}_u \quad \forall u \in \mathcal{U}, t \in \{\bar{t}_u, (n_f + 1)T - \bar{t}_u\} \quad (2.29)$$

ensures $\bar{b}_u(t) = 1$ if and only if UAV u has minimum velocity.

Proof. Due to constraint (2.6), the UAVs velocity is a linear function of its acceleration. Thus, the real time for reaching minimum velocity v_u with maximum acceleration \bar{a}_u is given by $\frac{v_u}{\bar{a}_u}$. Conversion into a number discrete time steps $\bar{t}_u \in \mathbb{N}$ leads to

$$\bar{t}_u := (n_f + 1) \left\lceil \frac{v_u}{\bar{a}_u \Delta t} \right\rceil. \quad (4)$$

Due to the objective function (3), the variable $\bar{b}_u(t)$ is set to zero to save fuel, if this is possible. To ensure that it is set to one \bar{t}_u time steps after the UAV starts to move or before it attempts to land, we relate it to $b_u(t)$. Then, $\bar{b}_u(t) = 1$ has to hold, if $b_u(t') = 1$ for all $t' \in \{t' - \bar{t}_u, t' + \bar{t}_u\}$. To relate all $2(\bar{t}_u + 1)$ binary variables $b_u(t')$ in this interval to a single binary decision, $2\bar{t}_u$ is subtracted leading to the desired equation (2.29). \square

To incorporate the new variable, the minimum velocity has to hold only \bar{t}_u time steps after takeoff. Thus, constraint (2.8) changes to

$$\underline{v}_u \bar{b}_u(\llbracket t \rrbracket) \leq \|\vec{v}_u(t)\|_2 \leq \bar{v}_u b_u(\llbracket t \rrbracket) \quad \forall u \in \mathcal{U}, t \in \mathcal{T}_f. \quad (2.8')$$

Accordingly, the fuel consumption equation (2.21) is adjusted to the new variable by

$$\sum_{i \in \mathcal{L}_u, j \in \mathcal{V}_u} s_{u,i,j}(t) = \bar{b}_u(t) \quad \forall u \in \mathcal{U}, t \in \mathcal{T}. \quad (2.21')$$

Otherwise, equations (2.21) and (2.22) would force any UAV that cannot accelerate to its minimum velocity in one timestep to stay on the ground.

Due to the physics of flight, a UAV slower than minimum velocity cannot ascend and therefore not take off. Thus, similar to the minimum velocity, the left part of equation (2.4) eliminates any UAV from the planning process if it cannot accelerate to its minimum velocity and ascend to the minimum altitude within a single time step. To avoid this, the variable $\bar{b}_u(t)$ also is incorporated into equation (2.4), leading to

$$\underline{h}_u \bar{b}_u(\llbracket t \rrbracket) \leq r_u^z(t) \leq \bar{h}_u b_u(\llbracket t \rrbracket) \quad \forall u \in \mathcal{U}, t \in \mathcal{T}_f. \quad (2.4')$$

We consider the minimum altitude small enough such that any UAV with minimum velocity can ascend to it within a fine time step.

Another occurring phenomenon in aviation is the altitude- and velocity-dependent change of flight dynamics due to decreasing thrust in higher altitudes caused by decreasing air temperature and pressure. It affects the maximum velocity as well as the maximum climb and descent rates. For the maximum velocity, altitude dependence is incorporated into the model by defining a maximum velocity $\bar{v}_{u,i}$ of UAV $u \in \mathcal{U}$ for every of its altitude bands $i \in \mathcal{L}_u$ and replace equation (2.8') by

$$\underline{v}_u \bar{b}_u(\llbracket t \rrbracket) \leq \|\vec{v}_u(t)\|_2 \leq \sum_{i \in \mathcal{L}_u} \bar{v}_{u,i} \sum_{j \in \mathcal{V}_u} s_{u,i,j}(\llbracket t \rrbracket) \quad \forall u \in \mathcal{U}, t \in \mathcal{T}_f. \quad (2.8'')$$

Besides this family of constraints, an altitude-dependent maximum velocity has to be taken into account in the calculation of the fuel consumption. By redefining parameter $\theta_{u,j}$ to $\theta_{u,i,j}$, describing the velocity of UAV $u \in \mathcal{U}$ in throttle band $j \in \mathcal{V}_u$ and altitude band $i \in \mathcal{L}_u$, equation (2.22) changes to

$$\sum_{i \in \mathcal{L}_u, j \in \mathcal{V}_u} \theta_{u,i,j} s_{u,i,j}(\llbracket t \rrbracket) = \|\vec{v}_u(t)\|_2 \quad \forall u \in \mathcal{U}, t \in \mathcal{T}_f. \quad (2.22')$$

For climb and descent rates, the velocity has to be taken into account, next to the altitude. In a similar way to the velocity, the related parameters change to $\bar{v}_{u,i,j}^{z,+}$ and $\bar{v}_{u,i,j}^{z,-}$, describing the maximum climb and descent rate of UAV $u \in \mathcal{U}$ for altitude band $i \in \mathcal{L}_u$ and throttle band $j \in \mathcal{V}_u$, respectively. Thereby, the upper bounds for the variables $v_u^{z,+}(t)$ and $v_u^{z,-}(t)$ are no longer constant. Thus, the new constraint for the upper limit of the descent rate is given by

$$v_u^{z,-}(t) \leq \sum_{i \in \mathcal{L}_u, j \in \mathcal{V}_u} s_{u,i,j}(t) \bar{v}_{u,i,j}^{z,-} \quad \forall u \in \mathcal{U}, t \in \mathcal{T}_f. \quad (2.30)$$

For the climb rate, the approach is a bit different since a constraint similar to (2.30) would reject any takeoff. Therefore, a new parameter $\bar{v}_u^{z,+}$ is introduced for the maximum climb rate at takeoff for every UAV $u \in \mathcal{U}$ and it is adjusted to get the maximum midair climb rates $\bar{v}_u^{z,+}$. The constraint, limiting the climb rate for every UAV, then has the form

$$v_u^{z,+}(t) \leq \bar{v}_u^{z,+} - \sum_{i \in \mathcal{L}_u, j \in \mathcal{V}_u} s_{u,i,j}(t) \left(\bar{v}_u^{z,+} - \bar{v}_{u,i,j}^{z,+} \right) \quad \forall u \in \mathcal{U}, t \in \mathcal{T}_f. \quad (2.31)$$

In model (2), the maximum acceleration of the UAVs is assumed to be constant in every situation. Thus, the computed flight trajectories are inaccurate since in practice the maximally allowed acceleration at the takeoff is significantly higher than during the flight. This results either in underestimation during the takeoff phase or overestimation when in midair. We follow the approach given in the Base of Aircraft Data [18] (BADA) of the Eurocontrol Experimental Centre. Therein, a reduction factor from takeoff thrust to cruise thrust applies with a value of $C_{Tcr} = 0.95$. It is incorporated into the model by changing equation (2.9) to

$$\bar{a}_u(t) (b_u(\|t\|) - 0.05\bar{b}_u(\|t\|)) \geq \|\bar{a}_u(t)\|_2 \quad \forall u \in \mathcal{U}, t \in \mathcal{T}_f. \quad (2.9')$$

2.2 Fuel-dependent Flight Dynamics

The flight dynamics in model (2) are independent of the mass of the considered UAVs, but this assumption only holds for electrical systems, where the weight of the battery is constant. For UAVs with liquid fuels, the mass affects the maximum velocity, maximum acceleration, maximum altitude, and fuel consumption rate [23] of an aircraft by weight reduction due to burned fuel. Since the portion of the fuel on the gross take-off weight of a UAV can go up to 43% [8], this has a great impact on the mission planning scenario. To include these fuel-dependent flight dynamics into the proposed model, several changes are necessary.

In terms of the altitude, we assume a linear dependency between the amount of remaining fuel and the reachable altitude. We expect the empty weight m_u of UAV u to include a small fuel reserve. Let UAV $u \in \mathcal{U}$ reach altitude $\bar{h}_u \left(1 - \frac{g_u(0)}{m_u + F_u}\right)$ for an initial amount of fuel $g_u(0)$ and its maximum altitude \bar{h}_u for $\varphi_u^{alt,1} g_u(0)$, with $\varphi_u^{alt,1} \in [0, 1)$. Additionally, there is an additive constant $\varphi_u^{alt,2} \in [0, 1]$ to achieve a more flexible initial altitude. The resulting linear function is displayed in figure 2 and gives the constraint

$$r_u^z(t) \leq \bar{h}_u \left(1 + \varphi_u^{alt,2} + \frac{\varphi_u^{alt,1} g_u(0) - g_u(t)}{(1 - \varphi_u^{alt,1})(m_u + F_u)} \right) \quad \forall u \in \mathcal{U}, t \in \mathcal{T}_f. \quad (2.32)$$

Besides, the right part of constraint (2.4') is still necessary to limit the reachable altitude to its maximum value and set the maximum altitude to zero when the UAV is on the ground.

To include the mass of the remaining fuel into the calculation of the velocity and the acceleration, we have the following proposition.

Proposition 2.2. *For any UAV $u \in \mathcal{U}$ and time step $t \in \mathcal{T}_f$, the linear approximations*

$$\|\bar{v}_u(t)\|_2 \leq \left(\varphi_u^{acc} \frac{g_u(t)}{F_u + m_u} + 1 \right) \bar{v}_{u,i} + \bar{V}_u \left(1 - \sum_{j \in \mathcal{V}_u} s_{u,i,j}(\|t\|) \right) \quad \forall i \in \mathcal{L}_u \quad (2.33)$$

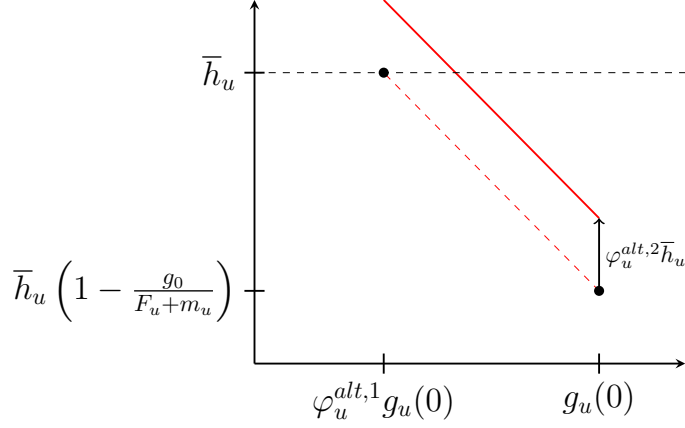


Figure 2: Linear dependency between the amount of fuel and the reachable altitude.

and

$$\|\vec{a}_u(t)\|_2 \leq \left(\varphi_u^{acc} \frac{g_u(t)}{F_u + m_u} + 1 \right) \bar{a}_u, \quad (2.34)$$

with $\bar{V}_u = \max_{i \in \mathcal{L}_u} \bar{v}_{u,i}$ and

$$\varphi_u^{acc} = (m_u + F_u) \frac{2 \left((F_u - 2m_u) \sqrt{m_u^2 + F_u m_u} + 2m_u^2 \right) - \frac{3}{2} F_u^2}{F_u^3}, \quad (5)$$

minimizes the quadratic error of the mass-dependent maximum velocity and acceleration, respectively.

Proof. We compare the given maximum velocity \bar{v}_u related to m_u with another velocity \tilde{v}_u for a UAV with more remaining fuel. Since the generated thrust of UAV $u \in \mathcal{U}$ is limited, it can reach a certain kinetic energy $E_u^{max} = \frac{1}{2} m_u \bar{v}_u^2$ for a given time. Thus, by energy preservation, we get the relation

$$\frac{1}{2} (m_u + g_u(t)) \tilde{v}_u^2 = \frac{1}{2} m_u \bar{v}_u^2 \quad \Rightarrow \quad \tilde{v}_u = \sqrt{\frac{m_u}{m_u + g_u(t)}} \bar{v}_u. \quad (6)$$

Using the equation $a = \frac{v}{t}$, in the same way the expression

$$\tilde{a}_u = \sqrt{\frac{m_u}{m_u + g_u(t)}} \bar{a}_u \quad (7)$$

can be derived. Since we consider the maximum velocity and acceleration in (6) and (7), we restrict on the positive solution of the respective square root. The non-linear factor for equations (6) and (7) is the same. Thus, we only have to perform one least squares approximation of the form

$$\min_{\varphi_u^{acc}} \int_0^{F_u} \left(\sqrt{\frac{m_u}{m_u + g_u(t)}} - \left(\varphi_u^{acc} \frac{g_u(t)}{m_u + F_u} + 1 \right) \right)^2 dg_u(t), \quad (8)$$

where we fix the absolute term of the linear function to 1 to ensure that the maximum velocity and acceleration is attained according to our assumption. The factor $\frac{1}{m_u + F_u}$ is applied to have a greater numerical value for φ_u^{acc} and thus avoid numerical issues. The solution of (8) gives the desired parameter φ_u^{acc} for the obtainable percentage of the maximum velocity and acceleration per unit of fuel for UAV $u \in \mathcal{U}$. Replacing the factor $b_u(\|t\|) - 0.05\bar{b}_u(\|t\|)$ by the computed linear function $\varphi_u^{acc} \frac{g_u(t)}{F_u + m_u} + 1$ in (2.9), it

gives the desired mass-dependent maximum acceleration (2.34) for every airborne UAV $u \in \mathcal{U}$ in time step $t \in \mathcal{T}_f$. In terms of the mass-dependent maximum velocity, the above approach is used and slightly modified since the altitude dependence in (2.8'') calls for the incorporation of an sufficiently large additive constant $\bar{V}_u \left(1 - \sum_{j \in \mathcal{V}_u} s_{u,i,j}(\lfloor t \rfloor)\right)$ with $\bar{V}_u = \max_{i \in \mathcal{L}_u} \bar{v}_{u,i}$ to avoid nonlinearities. This leads to the remaining equation (2.33). \square

In addition to equations (2.33) and (2.34) the constraints (2.8'') and (2.9') are still necessary to force the maximum velocity and acceleration to zero for grounded UAVs. The used approach is similar to the method in the BADA [18], except that we assume the UAV to reach maximum velocity and acceleration with only the fuel reserve incorporated in the empty weight. In terms of the fuel-dependent fuel consumption, a further parameter φ_u^{fuel} is necessary. It describes the additional fuel consumption for every remaining fuel unit at the previous time step and is incorporated as an additional factor into the constraint (2.20). To ensure that a UAV is consuming no fuel when landed, a distinction between the fuel calculation for a landed and a flying UAV is needed. Thus, the constraint (2.20) is replaced by

$$g_u(t+1) \leq F_u(1 - b_u(\lfloor t \rfloor)) + g_u(t) - \Delta t_f \left(\xi_u v_u^{z,+} + \sum_{i \in \mathcal{L}_u, j \in \mathcal{V}_u} \eta_{u,i,j} s_{u,i,j}(\lfloor t \rfloor) + \varphi_u^{fuel} g_u(t) \right) \quad \forall u \in \mathcal{U}, t \in \mathcal{T}_f^-, \quad (2.20i)$$

$$g_u(t+1) \geq -F_u(1 - b_u(\lfloor t \rfloor)) + g_u(t) - \Delta t_f \left(\xi_u v_u^{z,+} + \sum_{i \in \mathcal{L}_u, j \in \mathcal{V}_u} \eta_{u,i,j} s_{u,i,j}(\lfloor t \rfloor) + \varphi_u^{fuel} g_u(t) \right) \quad \forall u \in \mathcal{U}, t \in \mathcal{T}_f^-, \quad (2.20ii)$$

$$g_u(t+1) \leq g_u(t) + F_u b_u(\lfloor t \rfloor) \quad \forall u \in \mathcal{U}, t \in \mathcal{T}_f^-, \quad (2.20iii)$$

$$g_u(t+1) \geq g_u(t) - F_u b_u(\lfloor t \rfloor) \quad \forall u \in \mathcal{U}, t \in \mathcal{T}_f^-. \quad (2.20iv)$$

Applying these changes to the model, the flight dynamics of the UAVs are compromised since equation (2.19) ensures that every UAV takes off with maximum fuel, reducing the maximum altitude, velocity, and acceleration. Thus, equation (2.19) is dropped to make the amount of takeoff fuel variable and allow the UAVs to reduce the amount of initial fuel to achieve better flight dynamics. To ensure these fuel-saving aspects, the objective function (3) has to change to

$$\max_{u \in \mathcal{U}, w \in \mathcal{W}, t \in \mathcal{T}} S_w d_{u,w}(t) - \frac{1}{|\mathcal{U}|} \sum_{u \in \mathcal{U}} \frac{g_u(0)}{M^{fuel} F_u} - \frac{1}{T} \sum_{u \in \mathcal{U}, t \in \mathcal{T}} \frac{t}{M^{air}} b_u(t) + \frac{1}{|\mathcal{T}_f|} \sum_{u \in \mathcal{U}, t \in \mathcal{T}_f} \left(\frac{r_u^z(t)}{M^{alt}} - \frac{\|\vec{v}_u(t)\|_2}{M^{vel}} \right). \quad (3')$$

2.3 Range

In model (2), the maximum operating range ϱ_u is chosen constant, although it depends on the height A_u of the used antenna and the altitude $r_u^z(t)$ of the UAV. To achieve more a realistic setting, we deduce an altitude-dependent maximum range.

Proposition 2.3. *Let C be a constant with $C \geq \max_{u \in \mathcal{U}} \bar{h}_u$. Then the linear approximation*

$$\|\vec{r}_u(t) - \vec{G}_u\|_2 \leq \varrho^{alt} r_u^z(t) + \varrho^{init}, \quad (2.3')$$

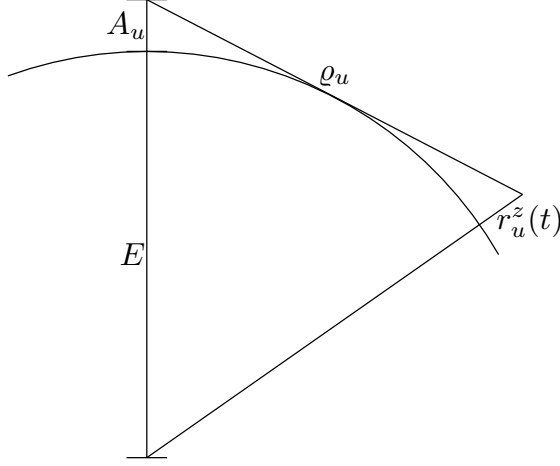


Figure 3: Maximal operating range ρ_u of a UAV for antenna height A_u and altitude $r_u^z(t)$.

with $\tilde{\rho}^{init} = \rho^{init} + \sqrt{2A_u E - A_u^2}$ and coefficients ρ^{alt} , ρ^{init} solving

$$\begin{aligned} \frac{2C^3}{3}\rho^{alt} + C^2\rho^{init} &= E^3 \left(\frac{\pi}{2} - \sin^{-1} \left(\frac{E-C}{E} \right) - \frac{E-C}{E} \sqrt{1 - \left(\frac{E-C}{E} \right)^2} \right), \\ &\quad - \frac{2E^3}{3} \left(1 - \left(\frac{E-C}{E} \right)^2 \right)^{\frac{3}{2}} \\ C^2\rho^{alt} + 2C\rho^{init} &= E^2 \left(\frac{\pi}{2} - \sin^{-1} \left(\frac{E-C}{E} \right) - \frac{E-C}{E} \sqrt{1 - \left(\frac{E-C}{E} \right)^2} \right), \end{aligned} \quad (9)$$

minimizes the quadratic error to the altitude-dependent maximum operating range at time step $t \in \mathcal{T}_f$.

Proof. The maximum range of UAV $u \in \mathcal{U}$ can be displayed as in figure 3. Applying the Pythagorean theorem, the maximum range is calculated by

$$\rho_u(r_u^z(t)) = \sqrt{2A_u E - A_u^2} + \sqrt{2E r_u^z(t) - (r_u^z(t))^2}, \quad u \in \mathcal{U}, t \in \mathcal{T}_f, \quad (10)$$

where E is the radius of the earth and A_u is the height of the antenna.

Due to the nonlinearity of this expression, we use the continuous least squares method to find the best approximation in terms of a linear function $f(x) = \rho^{alt}x + \rho^{init}$. Since the antenna height A_u is constant, the first term in (10) is an additive constant and only shifts the whole function. Thus it can be neglected in the least squares approximation, leading to the problem

$$\min_{\rho^{alt}, \rho^{init}} \int_0^C \left(\sqrt{2E r_u^z(t) - (r_u^z(t))^2} - (\rho^{alt} r_u^z(t) + \rho^{init}) \right)^2 dr_u^z(t), \quad (11)$$

with $C \geq \max_{u \in \mathcal{U}} \bar{h}_u$ representing a sufficiently large altitude as upper limit of the integral. By integration and solution of the remaining minimization problem, the parameters ρ^{alt} and ρ^{init} are given by (9). Finally, the constant maximum operating range ρ_u in (2.3) is replaced by the linear function $\rho^{alt} r_u^z(t) + \rho^{init}$ to obtain (2.3'). \square

2.4 Restricted Airspaces

Equations (2.15) and (2.16) in model (2) allow to incorporate restricted airspaces for the UAVs, but only cubic ones which are parallel to the coordinate axes. To compare the respective coordinates of UAV $u \in \mathcal{U}$ and the restricted airspace $q \in \mathcal{Q}$ at time step $t \in \mathcal{T}$ and report if it is inside the area, two binary variables $\underline{f}_{u,q}^i, \bar{f}_{u,q}^i$ are necessary for every

coordinate direction $i \in \{x, y, z\}$, one per side. Using this approach, also more complex restricted airspaces can be modeled by a union of these cubic ones, but only at the expense of many additional binary variables.

To describe restricted airspaces by arbitrary polyhedrons, we assume its N_q^Q describing hyperplanes to have coordinate form with normal vector $\vec{c}_{q,i}(t)$ and right-hand side $c_{q,i}^{rhs}(t)$ for $i = 1, \dots, N_q^Q$ and $q \in \mathcal{Q}$. Thus, every restricted airspace $q \in \mathcal{Q}$ is represented by

$$\mathcal{A}_q^Q(t) = \left\{ \vec{x} \in \mathbb{R}^3 \mid \vec{c}_{q,i}(\llbracket t \rrbracket) \cdot \vec{x} \leq c_{q,i}^{rhs}(\llbracket t \rrbracket), i = 1, \dots, N_q^Q \right\}. \quad (12)$$

Similar to the parameters, the related binary variables $f(t)$ are redefined to $f_{u,q,i}(t)$, with $f_{u,q,i}(t) = 1$ if UAV $u \in \mathcal{U}$ is outside of the restricted airspace $q \in \mathcal{Q}$ regarding hyperplane $i = 1, \dots, N_q^Q$ at time step $t \in \mathcal{T}$, and $f_{u,q,i}(t) = 0$ otherwise. Then equations (2.15) and (2.16) are replaced by

$$\vec{c}_{q,i}(\llbracket t \rrbracket) \cdot \vec{r}_u(t) \geq c_{q,i}^{rhs}(\llbracket t \rrbracket) - M^{dist} (1 - f_{u,q,i}(\llbracket t \rrbracket)) \quad \forall u \in \mathcal{U}, q \in \mathcal{Q}, i = 1, \dots, N_q^Q, t \in \mathcal{T}_f, \quad (2.15')$$

$$\sum_{i=1}^{N_q^Q} f_{u,q,i}(t) \geq 1 \quad \forall u \in \mathcal{U}, q \in \mathcal{Q}, t \in \mathcal{T}, \quad (2.16')$$

providing a more general approach to model restricted convex airspaces with again one binary variable per side.

2.5 Wind

In the basic model (2), the wind is assumed to blow constantly everywhere within the considered area. By introducing the fine time steps, the wind can change in every fine time step $t \in \mathcal{T}_f$. To allow a more accurate influence of weather conditions, we want to include the possibility of different wind zones within the mission area. But this comes with the restriction that wind changes only in time steps $t \in \mathcal{T}$. For simplicity, the computation of the position (2.5) is modified to

$$r_u^i(t+1) = r_u^i(t) + \Delta t_f (v_u^i(t) + \tilde{w}_u^i(t)) + \frac{(\Delta t_f)^2}{2} a_u^i(t) \quad \forall u \in \mathcal{U}, t \in \mathcal{T}_f^-, i \in \{x, y\}, \quad (2.5')$$

where $\tilde{w}_u^i(t)$ is the influence of wind for UAV $u \in \mathcal{U}$ in coordinate direction $i \in \{x, y\}$ at time step $t \in \mathcal{T}_f^-$.

As a first approach, altitude-dependent wind zones could be added since the wind intensity and its direction can change with increasing altitude, e.g., the jetstream has to be taken into account for mission planning in altitudes between 8 to 12 kilometers. To incorporate this into our model, the wind vector $\vec{w}_l(t) = (w_l^x(t), w_l^y(t)) \in \mathbb{R}^2$ is now defined for every altitude band $l \in \mathcal{L}_u$. Since the variable $s_{u,i,j}(t)$ cannot change in every fine step, there is a discretization error between two time steps if the altitude layer is changed. To reduce its influence, we consider a convex combination of the wind between time steps $t, t + n_f + 1 \in \mathcal{T}$ at every fine time step $t \in \mathcal{T}_f$. Thus, the influence of wind is calculated by

$$\tilde{w}_u^i(t) = \sum_{l \in \mathcal{L}_u, j \in \mathcal{V}_u} \left((1 - \mu) w_l^i(\llbracket t \rrbracket) s_{u,i,j}(\llbracket t \rrbracket) + \mu w_l^i(\lceil \lceil t \rceil \rceil) s_{u,i,j}(\lceil \lceil t \rceil \rceil) \right) \quad \forall u \in \mathcal{U}, t \in \mathcal{T}_f^-, i \in \{x, y\}, \quad (13)$$

with $\mu = \frac{t \bmod (n_f+1)}{n_f+1}$ and $\lceil t \rceil = \lfloor t \rfloor + n_f + 1$. But this method requires again constant wind direction within every altitude band over the whole mission area.

To overcome this drawback, a second approach is possible. In the same way as for the restricted airspaces in section 2.4, a set \mathcal{P} of wind zones is defined, described by N_p^P hyperplanes

$$\mathcal{A}_p^P(t) = \left\{ \vec{x} \in \mathbb{R}^3 \mid \vec{n}_{p,i}(\lfloor t \rfloor) \cdot \vec{x} \leq n_{p,i}^{rhs}(\lfloor t \rfloor), i = 1, \dots, N_p^P \right\}, \quad (14)$$

with normal vectors $\vec{n}_{p,i}(t)$ and right-hand sides $n_{p,i}^{rhs}(t)$.

Furthermore, new binary variables $w_{u,p,i}(t) \in \{0, 1\}$ are introduced with $w_{u,p,i}(t) = 1$, if UAV $u \in \mathcal{U}$ is within wind zone $p \in \mathcal{P}$ regarding hyperplane $i \in \mathcal{A}_p^P$ at time step $t \in \mathcal{T}$. In contrast to the restricted airspaces, now additional constraints and an auxiliary binary variable $\omega_{u,p}(t)$ are necessary to map the variables $w_{u,p,i}(t)$ to a single binary decision and to ensure that wind is only taken into account when UAV $u \in \mathcal{U}$ is in midair. Therefore, the decision if UAV u is affected by wind zone p at time step t is modeled by

$$\vec{n}_{u,p,i}(\lfloor t \rfloor) \cdot \vec{r}_u(t) \geq n_{p,i}^{rhs}(\lfloor t \rfloor) - M^{dist} w_{u,p,i}(\lfloor t \rfloor) \quad \forall u \in \mathcal{U}, p \in \mathcal{P}, i = 1, \dots, N_p^P, t \in \mathcal{T}_f, \quad (2.35)$$

$$\sum_{i=1}^{N_p^P} w_{u,p,i}(t) \leq N_p^P + \omega_{u,p}(t) - 1 \quad \forall u \in \mathcal{U}, p \in \mathcal{P}, t \in \mathcal{T}, \quad (2.36)$$

$$\sum_{i=1}^{N_p^P} w_{u,p,i}(t) \geq N_p^P \omega_{u,p}(t) \quad \forall u \in \mathcal{U}, p \in \mathcal{P}, t \in \mathcal{T}, \quad (2.37)$$

$$\sum_{p \in \mathcal{P}} \omega_{u,p}(t) \leq |\mathcal{P}| b_u(t) \quad \forall u \in \mathcal{U}, t \in \mathcal{T}. \quad (2.38)$$

Analogue to the first approach, the variable $w_{u,p}(t)$ can only change at time step $t \in \mathcal{T}$. Thus, the convex combination with \tilde{t} is applied again and the influence of wind is calculated by

$$\tilde{w}_u^i(t) = \sum_{p \in \mathcal{P}} (1 - \mu) w_p^i(\lfloor t \rfloor) \omega_{u,p}(\lfloor t \rfloor) + \mu w_p^i(\lceil t \rceil) \omega_{u,p}(\lceil t \rceil) \quad \forall u \in \mathcal{U}, t \in \mathcal{T}_f^-, i \in \{x, y\}, \quad (2.39)$$

where again $\mu = \frac{t \bmod (n_f+1)}{n_f+1}$ and $\lceil t \rceil = \lfloor t \rfloor + n_f + 1$. For this approach, the number of binary variables within the model increases by $\sum_{p \in \mathcal{P}} (|A_p^P| + 1)$ per time step and UAV.

3 Collision Avoidance

Compliance with safety distances in aviation is crucial due to the disastrous consequences of its failure. Therefore, the parts of a planning model computing collision-free flight trajectories should be examined excessively. In the following, we consider a two dimensional and a three dimensional setting to examine the modelled collision avoidance (2.17) and (2.18).

A class of two-dimensional benchmark instances, called Random Circle Problems (RCPs) [7], has a wide application in collision avoidance and conflict resolution. In this problem class, a set of aircrafts is randomly arranged on a circle. At the beginning, all UAVs maintain the safety distances, head towards the circles center, and have their respective destination on its opposite side. The deviation from the shortest connection is

minimized for every participant. With an increasing number of aircrafts, it is a challenging problem to conflict resolution approaches due to its fast increasing violations of the safety distance if no countermeasures are taken.

We adapt these benchmark instances to our setting, assuming every participating UAV has the same technical characteristics. Thus, there are no waypoints and the start locations of the participating UAVs are distributed randomly along a circle of radius r^{RCP} , with their respective end location on the opposite side. The operating range is neglected since every UAV must be able to reach its end location. Thus, the whole circle is within its operating range. In the beginning, every UAV is heading towards the center of the circle and all safety distances are ensured. To incorporate this into the model, a new constraint

$$v_u(0) = \gamma_u \cdot \vec{1} \cdot \left(\vec{C} - \vec{R}_u^0 \right) \quad \forall u \in \mathcal{U}, \quad (15)$$

is added, where \vec{C} is the location of the center of the considered circle and the new variable γ_u scales the given direction to ensure the limits of the velocity.

Due to the absence of waypoints and the altitude, many constraints can be neglected and also many binary variables are unnecessary or must be redefined, i.e., $s_{u,i,j}(t)$ changes to $s_{u,j}(t)$ indicating whether UAV $u \in \mathcal{U}$ is within throttle band $j \in \mathcal{V}_1$ at time step $t \in \mathcal{T}$ and the variables $b_u(t)$ and $\bar{b}_u(t)$ are substituted by $b_u^-(t)$ since all UAVs start in midair and have to stop at their end location.

We minimize the deviation of the shortest connection by the number of necessary time steps T^{min} , such that every UAV reaches its respective end location. This number is not known a priori and increases the more UAVs are participating. Only a lower bound \underline{T}^{min} is given by the number of time steps it takes for a single UAV to fly along the diameter of the circle with maximum velocity. Setting T to a sufficiently large value and read T^{min} from the optimal solution can be an ineffective way since the number of constraints and variables is time-dependent, leading to a possibly too large model. Therefore, we use an approach from [2], solving the RCP sequentially for an increasing number of time steps, starting with $T = \underline{T}^{min}$, until a feasible solution is found or its existence cannot be determined within a given computation time. This procedure has the advantage of working without any objective function since the first found feasible solution gives the value of T^{min} .

To ensure that the safety distances are observed at every time step, it has to hold

$$\Delta t \leq \frac{\max_{i \in \{x,y\}} \varepsilon^i}{\bar{V}_1}, \quad (16)$$

where $\bar{V}_1 = \max_{i \in \mathcal{L}_1} \bar{v}_{1,i}$ is again the maximum of the altitude-dependent maximum velocities of the first UAV. Due to the assumption of identical technical characteristics of all participating UAVs, the first UAV can be chosen without loss of generality. Without condition (16), a pair of UAVs, complying with the safety distance between them, could swap their positions within one time step by flying through each other. The resulting resolution of the time is sufficient to obtain smooth trajectories. Thus, we renounce on fine time steps in this case.

The following result gives a heuristical solution for the two-dimensional RCP.

Proposition 3.1. *Consider the two-dimensional RCP with center $\vec{C} \in \mathbb{R}^2$, radius $r^{RCP} \in \mathbb{R}_+$, safety distances $\vec{\varepsilon} \in \mathbb{R}_+^2$, time step length $\Delta t \in \mathbb{R}_+$, $n \in \mathbb{N}$ participating UAVs, and $\bar{v} \in \mathbb{R}_+$ their maximum velocity. Then it holds*

$$T^{min} \leq \left\lceil \frac{2r^{RCP} + (\pi - 2) \|\vec{C} - \vec{r}_n(t')\|}{\bar{v} \Delta t} \right\rceil, \quad (17)$$

with

$$t' = \min_{t \in \mathbb{Z}_+} \{ \|\vec{r}_{u_1}(t+1) - \vec{r}_{u_2}(t+1)\| \leq \|\vec{\varepsilon}'\| \mid u_1, u_2 \in \{1, \dots, n\}; u_1 < u_2 \}. \quad (18)$$

Proof. Every UAV starts at its random starting location and heads towards the center \vec{C} with maximum speed. To avoid conflicts near the center \vec{C} , all UAVs are assigned to a smaller circle with center \vec{C} and radius $r^{ub} \leq r^{RCP}$ before the first conflict would occur. Along this smaller circle, the UAVs rotate around its center on a semicircle and then fly to their respective end locations. This approach generates a feasible solution if the safety distances are observed during the rotation. Therefore, it is necessary to ensure at least the distance $\|\vec{\varepsilon}'\|$ between any pair of UAVs. Let t' be the last time step with this property. It is computed by

$$t' = \min_{t \in \mathbb{Z}_+} \{ \|\vec{r}_{u_1}(t+1) - \vec{r}_{u_2}(t+1)\| \leq \|\vec{\varepsilon}'\| \mid u_1, u_2 \in \{1, \dots, n\}; u_1 < u_2 \}. \quad (19)$$

The radius r^{ub} is then given by $\|\vec{C} - \vec{r}_n(t')\|$, where the position of any UAV at time step t' can be chosen since they all have equal distance to the center. Without loss of generality, we take the position of UAV n . For the described solution, every UAV must fly a distance of $2(r^{RCP} - r^{ub}) + \pi r^{ub}$ units to reach its end location. Thus, there are

$$T = \left\lceil \frac{2r^{RCP} + (\pi - 2)r^{ub}}{\bar{v}\Delta t} \right\rceil \quad (20)$$

time steps necessary to complete this trajectory. Substitution of r^{ub} leads to the upper bound of T^{min} given in (17). \square

Furthermore, the quality of the described heuristic solution can be calculated.

Corollary 3.2. *For the two-dimensional RCP with minimum number of time steps \underline{T}^{min} , it holds*

$$1 \leq \frac{T^{min}}{\underline{T}^{min}} \leq \frac{\pi}{2}. \quad (21)$$

Proof. In the worst case, there are two UAVs $u_1, u_2 \in \mathcal{U}$ starting with $\|\vec{R}_{u_1}^0 - \vec{R}_{u_2}^0\| = \|\vec{\varepsilon}'\|$. Then it follows $r^{ub} = r^{RCP}$ and the trajectory of every UAV is πr^{RCP} . Since all UAVs have the same constant maximum velocity \bar{v} , it holds $\underline{T}^{min} = 2r^{RCP}\bar{v}$ and the number of time steps T^{min} depends only on the radius r^{RCP} , leading to $T^{min} = \pi r^{RCP}\bar{v} = \frac{\pi}{2}\underline{T}^{min}$. Thus, in a general setting the desired estimate (21) is obtained by combining the definition of \underline{T}^{min} with the described worst case and rearranging it. \square

For the case of evenly distributed UAVs, the result of proposition 3.1 can be computed without the knowledge of t' .

Corollary 3.3. *Consider the Circle Problem with $n \in \mathbb{N}$ evenly distributed UAVs with maximum velocity $\bar{v} \in \mathbb{R}_+$, radius $r^{RCP} \in \mathbb{R}_+$, safety distances $\vec{\varepsilon}' \in \mathbb{R}_+^2$, and time step length $\Delta t \in \mathbb{R}_+$. Then it holds*

$$T^{min} \leq \left\lceil \frac{2r^{RCP} + \frac{(\pi-2)}{2\sin(\frac{\pi}{n})}\|\vec{\varepsilon}'\|}{\bar{v}\Delta t} \right\rceil. \quad (22)$$

Proof. In the evenly distributed case, every pair of UAVs has the same distance. Thus, their start locations are the corners of a regular polygon with circumradius r^{RCP} . Since all UAVs head towards the center with the same velocity, they stay corner points of a regular

polyhedron with decreasing side length. The radius r^{ub} of the smaller circle is then the circumradius of a regular polyhedron with n corners and side length ε^z . It is computed by

$$r^{ub} = \frac{\|\varepsilon^z\|}{2 \sin\left(\frac{\pi}{n}\right)} \quad (23)$$

Substituting this term into (20) gives the upper bound (22). \square

The model in the two-dimensional case is given by the constraints (2.1), (2.2), (2.5'), (2.6), (2.8'), (2.9'), (2.11), (2.17), (2.18), (2.20i) – (2.20iv), (2.21), (2.22), (2.33), (2.34), and (15), where all terms with $v_u^{z,+}(t)$ are neglected, due to the absence of altitude changes. Furthermore, the variables $b_u(t)$ and $\bar{b}_u(t)$ have to be substituted by $b_u^-(t)$ since all UAVs start in midair and should only stop at their respective end locations.

Since in ordinary air traffic the aircrafts are not restricted to a single altitude and to fully evolve the potential of our model, we extend the concept of RCPs into three dimensions. Therefore, minimum and maximum altitudes \underline{h} and \bar{h} are incorporated as lower and upper bound of the altitude $r_u^z(t)$ of every UAV $u \in \mathcal{U}$ at time step $t \in \mathcal{T}_f$, respectively. All UAVs are positioned analog to the two-dimensional case, but with initial altitude $R^{0,z} \in [\underline{h}, \bar{h}]$.

The result of proposition 3.1 can also be adapted for the three-dimensional RCP.

Proposition 3.4. *Consider the three-dimensional RCP with center $\vec{C} \in \mathbb{R}^3$, radius $r^{RCP} \in \mathbb{R}_+$, minimum and maximum altitude \underline{h} and \bar{h} , safety distances $\varepsilon^z \in \mathbb{R}_+^3$, and time step length $\Delta t \in \mathbb{R}_+$. Let $n^l = \lfloor \frac{\bar{h}-\underline{h}}{\varepsilon^z} \rfloor$ and the sets $\mathcal{U}_1, \dots, \mathcal{U}_{n^l}$ be a partition of $\mathcal{U} = \{1, \dots, n\}$. Furthermore, every participating UAV has maximum velocity $\bar{v} \in \mathbb{R}_+$, maximum climb and descent rate $\bar{v}^{z,+}$ and $\bar{v}^{z,-}$, and initial altitude $R^{0,z}$. Then it holds*

$$T^{min} \leq \max_{i \in \{1, \dots, n^l\}} \left\{ \left\lceil \frac{2r^{RCP} + (\pi - 2)\|\vec{C} - \vec{r}_n(t'_i)\|}{\bar{v}\Delta t} \right\rceil + \left\lceil \frac{|R^{0,z} - \underline{h} + (i-1)\varepsilon^z|}{\bar{v}^{z,+}\Delta t} \right\rceil + \left\lceil \frac{|R^{0,z} - \underline{h} + (i-1)\varepsilon^z|}{\bar{v}^{z,-}\Delta t} \right\rceil \right\}, \quad (24)$$

with

$$t'_i = \min_{t \in \mathbb{Z}_+} \{ \|\vec{r}_{u_1}(t+1) - \vec{r}_{u_2}(t+1)\| \leq \|\varepsilon^z\| \mid u_1, u_2 \in \mathcal{U}_i; u_1 < u_2 \} \quad \forall i \in \{1, \dots, n^l\}. \quad (25)$$

Proof. For the given altitude range $[\underline{h}, \bar{h}]$ and vertical safety distance ε^z , it is possible to stack $n^l = \lfloor \frac{\bar{h}-\underline{h}}{\varepsilon^z} \rfloor$ UAVs one above each other at the same x - and y -coordinates. Thus, every partition $\{\mathcal{U}_i\}_{i \in \{1, \dots, n^l\}}$ of the set $\mathcal{U} = \{1, \dots, n\}$ decomposes the three-dimensional RCP into n^l two-dimensional RCPs considering only the UAVs \mathcal{U}_i , respectively. According to this, the number of time steps to perform the three-dimensional trajectory of every UAV u is the sum of the number of time steps for its trajectory in the two-dimensional problem and the number of time steps necessary for the altitude changes.

To arrange all two-dimensional RCPs into the altitude range $[\underline{h}, \bar{h}]$, one of them is located at the lower or upper altitude limit and the vertical distance between two of them is at least ε^z . Without loss of generality, we assign the problem considering the UAVs of subset \mathcal{U}_1 to the altitude \underline{h} . Then, the necessary number of time steps for the altitude changes of every UAV $u \in \mathcal{U}_i$ are computed by

$$T_i^z = \left\lceil \frac{|R^{0,z} - \underline{h} + (i-1)\varepsilon^z|}{\bar{v}^{z,+}\Delta t} \right\rceil + \left\lceil \frac{|R^{0,z} - \underline{h} + (i-1)\varepsilon^z|}{\bar{v}^{z,-}\Delta t} \right\rceil \quad \forall i \in \{1, \dots, n^l\}. \quad (26)$$

Table 6: Data for the UAV technical parameters according to [8].

Description	Parameter	Unit	UAV-1	UAV-2
Minimum velocity	\underline{v}_u	$\frac{\text{km}}{\text{h}}$	130	167
Maximum velocity	\bar{v}_u	$\frac{\text{km}}{\text{h}}$	232	204
Military static thrust at s/l	F_u^N	kp	1250	64
Maximum initial climb rate	$\bar{v}_u^{z,+0}$	$\frac{\text{m}}{\text{s}}$	8	2
Maximum fuel	F_u	kg	2000	150
Fuel surplus for climbing	ξ_u	$\frac{\text{kg}}{\text{min}}$	0.2	0.02
Empty weight	m_u	kg	4000	540

Thus, the number of necessary time steps in the three-dimensional case is computed by

$$T_i = \left\lceil \frac{2r^{RCP} + (\pi - 2)\|\vec{C} - \vec{r}_n(t')\|}{\bar{v}\Delta t} \right\rceil + \left\lceil \frac{|R^{0,z} - \underline{h} + (i-1)\varepsilon^z|}{\bar{v}^{z,+}\Delta t} \right\rceil + \left\lceil \frac{|R^{0,z} - \underline{h} + (i-1)\varepsilon^z|}{\bar{v}^{z,-}\Delta t} \right\rceil \forall i \in \{1, \dots, n_l\}, \quad (27)$$

with t' from proposition 3.1. The maximum of these T_i is the desired upper bound (24). \square

The model in the two-dimensional case is given by the constraints (2.1), (2.2), (2.5') – (2.9'), (2.11), (2.17), (2.18), (2.20i) – (2.20iv), (2.21) – (2.23), (2.30), (2.31), (2.33), (2.34), (15), and the constraint

$$\underline{h} \leq r_u^z(t) \leq \bar{h} \quad \forall u \in \mathcal{U}, t \in \mathcal{T}_f. \quad (28)$$

Similar to the two-dimensional case, the variables $b_u(t)$ and $\bar{b}_u(t)$ are substituted by $b_u^-(t)$.

4 Computational Results

To test the derived results, we apply the extended model (2) with objective (3') to different instances considering real-world UAVs. These are:

UAV-1. Heron TP UAV [Eitan] - Israel (Air Force), since 2012.

UAV-2. RQ-5A Hunter UAV - United States (Army), since 1996.

The data for the technical parameters of the UAVs are taken from [8] and can be found in Table 6 to Table 8.

As length of one time step, $\Delta t = 0.1\text{h}$ is assumed. Regarding the maximum operating range, we choose in (9) $C^{range} = 15\text{km}$, $E = 6371\text{km}$, and $A_u = 0.005\text{km}$ for all $u \in \mathcal{U}$. Thus, we obtain the optimal values $m := 23.30$ and $\tilde{n} := 116.61$, leading to the linear approximation displayed in figure 4. For the altitude and throttle dependent climb rate we assume $\bar{v}_{u,i,j}^{z,+} = \bar{v}_u^{z,+0}$ for all UAVs $u \in \mathcal{U}$, altitude bands $i \in \mathcal{L}_u$, and throttle bands $j \in \mathcal{V}_u$.

The operational range $\delta_{u,w}$ of UAV $u \in \mathcal{U}$ to waypoint $w \in \mathcal{W}$ is set to a value within the second highest altitude band to reject the UAVs staying at maximum altitude all the time. According to this, we choose the values $\delta_{1,w} = 10\text{km}$ and $\delta_{2,w} = 3\text{km}$.

Table 7: Altitude and throttle band related data of UAV-1 according to [8].

Altitude- Throttle band	Altitude (in km)	velocity (in $\frac{\text{km}}{\text{h}}$)	descend rate (in $\frac{\text{m}}{\text{s}}$)	fuel cons. (in $\frac{\text{kg}}{\text{min}}$)
Altitude band 1 loiter speed	0.001– 3.658	130	8	2.08
Altitude band 1 cruise speed	0.001– 3.658	204	24	2.60
Altitude band 1 military speed	0.001– 3.658	232	24	5.23
Altitude band 2 loiter speed	3.658– 7.315	130	8	1.53
Altitude band 2 cruise speed	3.658– 7.315	204	24	1.91
Altitude band 2 military speed	3.658– 7.315	232	24	3.85
Altitude band 3 loiter speed	7.315– 10.972	130	8	1.06
Altitude band 3 cruise speed	7.315– 10.972	204	24	1.33
Altitude band 3 military speed	7.315– 10.972	232	24	2.66
Altitude band 4 loiter speed	10.972– 13.716	130	8	0.70
Altitude band 4 cruise speed	10.972– 13.716	204	24	0.88
Altitude band 4 military speed	10.972– 13.716	232	24	1.78

Table 8: Altitude and throttle band related data of UAV-2 according to [8].

Altitude- Throttle band	Altitude (in km)	velocity (in $\frac{\text{km}}{\text{h}}$)	descend rate (in $\frac{\text{m}}{\text{s}}$)	fuel cons. (in $\frac{\text{kg}}{\text{min}}$)
Altitude band 1 loiter speed	0.001– 3.658	167	2	0.19
Altitude band 1 cruise speed	0.001– 3.658	194	6	0.23
Altitude band 1 military speed	0.001– 3.658	204	6	0.44
Altitude band 2 loiter speed	3.658– 4.572	167	2	0.14
Altitude band 2 cruise speed	3.658– 4.572	194	6	0.17
Altitude band 2 military speed	3.658– 4.572	204	6	0.32

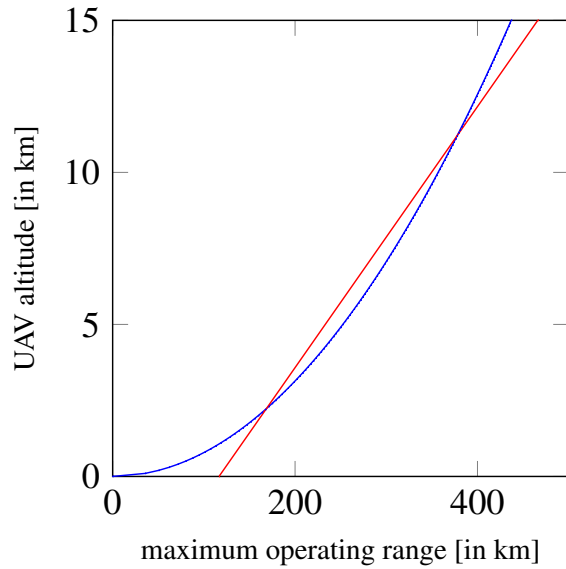


Figure 4: Linear approximation of the nonlinear maximum operating range function for antenna height $A_u = 0$.

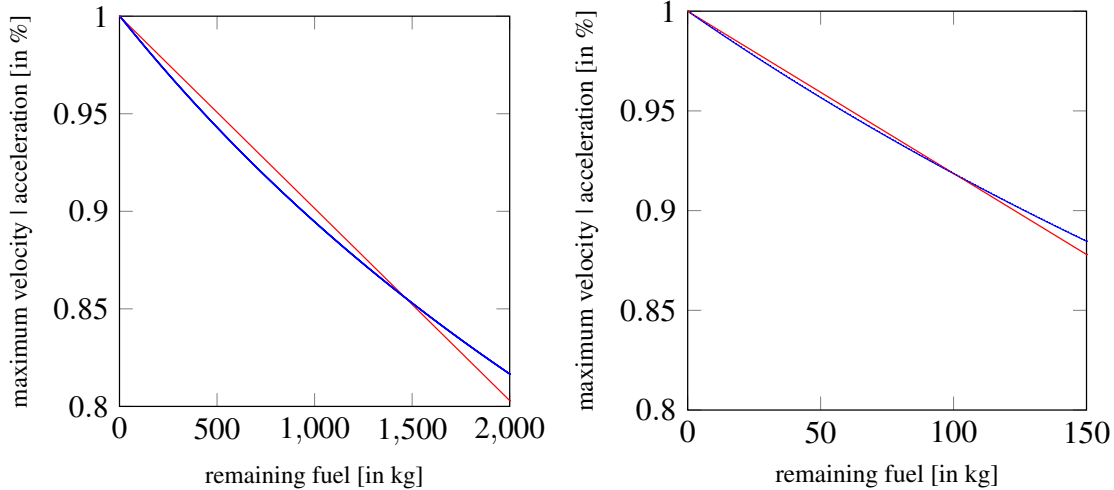


Figure 5: Least squares approximation of the non-linear factor for the maximum velocity and acceleration of UAV-1 (*left*) and UAV-2 (*right*)

The maximum acceleration \bar{a}_u of UAV $u \in \mathcal{U}$ is not provided by [8], but it gives a value for the military static thrust at starting or landing. In these processes, the maximum possible acceleration of the aircraft is used [23], so we use it as an upper bound for every time step. To compute the acceleration related to the given thrust, the second of Newton's axioms $F = ma$ is chosen, rearranged to get a , and the thrust, converted to Newton, is put in. Combined with the conversion factor from $\frac{\text{m}}{\text{s}^2}$ to $\frac{\text{km}}{\text{h}^2}$, this yields the formula

$$\bar{a}_u = 12960 \frac{9.807 F_u^N}{m_u}. \quad (29)$$

Applied to the considered UAVs, it gives $\bar{a}_1 = 26478.9 \frac{\text{km}}{\text{h}^2}$ and $\bar{a}_2 = 11788.87 \frac{\text{km}}{\text{h}^2}$.

Equation (5) with the respective values of every UAV $u \in \mathcal{U}$ results in the parameter values $\varphi_1^{acc} = -0.591$ for UAV-1 and $\varphi_2^{acc} = -0.554$ for UAV-2, displayed in figure 5. For the constraint of mass-dependent maximum reachable altitude (2.32), we choose $\varphi_u^{alt,1} = 0$ and $\varphi_u^{alt,2} = 1$ for all $u \in \mathcal{U}$. In absence of data, we set $\varphi_u^{fuel} = 0$.

For the weights of the objective function M^i , $i \in \{air, fuel, vel, alt\}$ it has to hold

$$\frac{1}{|T_f|} \left(\sum_{u \in \mathcal{U}} \frac{g_u(0)}{M^{fuel}} + \sum_{u \in \mathcal{U}, t \in T_f} \left(\frac{t}{(n_f + 1)M^{air}} b_u(\|t\|) + \frac{\|\vec{v}_u(t)\|_2}{M^{vel}} \right) \right) < \underline{S}, \quad (30)$$

$$\sum_{u \in \mathcal{U}, t \in T_f} \frac{r_u^z(t)}{M^{alt}|T_f|} < \underline{S}, \quad (31)$$

with $\underline{S} = \min_{w \in \mathcal{W}} \{S_w\}$ to ensure that visiting a waypoint is always preferred. In this work, we choose $M^{air} = 10^2$, $M^{fuel} = 10^4$, $M^{vel} = 10^5$, $M^{alt} = 10^4$. Furthermore, we assume the sufficiently large constant $M^{dist} = 10^3$ and set $S_w = 1$ for all $w \in \mathcal{W}$.

All instances were generated with the modeling language AMPL (Version: 20200501) and solved with GUROBI 9.0.2 [11] on an Apple MacMini running an IntelCore i7 at 3.20 GHz clock speed and 64 GB RAM, with the relative and absolute gap set to 0 and default settings otherwise.

4.1 CPU Time Analysis

In this section, we examine the influence of the discretization and approximation techniques to the computation time of the problem. With the use of a more detailed approach,

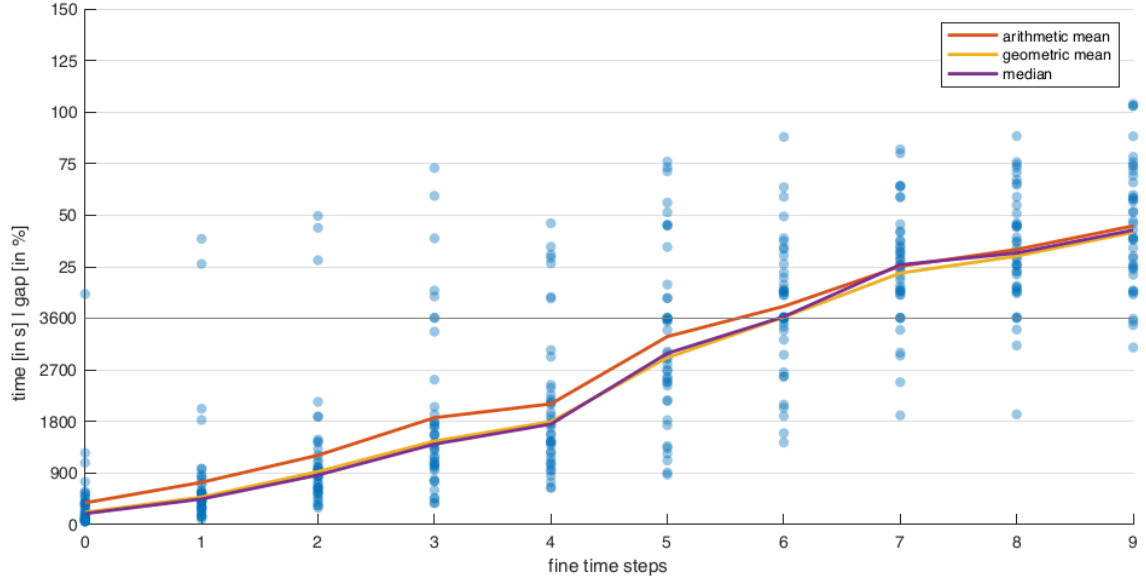


Figure 6: Solution time depending on the number of fine time steps.

the resulting problem becomes more complex and its computation time rises. Since we apply the state-of-the-art solver GUROBI, we find the instance sizes that can be solved within a given time limit.

To examine the influence of fine time steps on the solution time, we generate 41 instances with 15 waypoints, a single UAV, 40 time steps, and two restricted airspaces and vary the number of fine time steps from 0 to 9. The results in figure 6 show, that the average computation time increases with a larger number of fine time steps. To solve 90% of the given instances within the considered time limit, at most two fine time steps can be used. The total amount of CPU time for solving all 410 instances was 922,686 seconds.

A comparison of the computed flight trajectories of a single instance for different numbers of fine time steps is shown in figure 7. One can see, that the optimal trajectory gets less crooked for an increasing number of fine time steps since the UAV has more possibilities to change its velocity and acceleration. At the same time, the differences between the computed trajectories become smaller, thus it suggests to use not too many fine time steps to save computation time.

4.2 Special Instances

In the following experiments, we apply the model to specially designed instances to examine some of its aspects in detail. For the effect of wind to the optimal flight trajectories, we compare the optimal solutions of an instance with and without the presence of wind. Furthermore, the altitude-dependent operating range approach the mass-dependent flight dynamics are discussed.

4.2.1 Influence of Wind Zones

We consider an instance with 10 waypoints, two UAVs, 25 time steps with 4 fine time steps each, and three wind zones. Their respective area and wind velocity are given in table 9. The first wind zone displays the jetstream on the northern hemisphere, while the other two describe local weather phenomena with a heavy storm to emphasize its influence on the UAVs, although real UAVs would stay on the ground in this situation. In absence of wind, the total amount of CPU time to solve the instance was 280 seconds, while in presence of wind the computation time increased to 5,263 seconds. The optimal flight trajectories

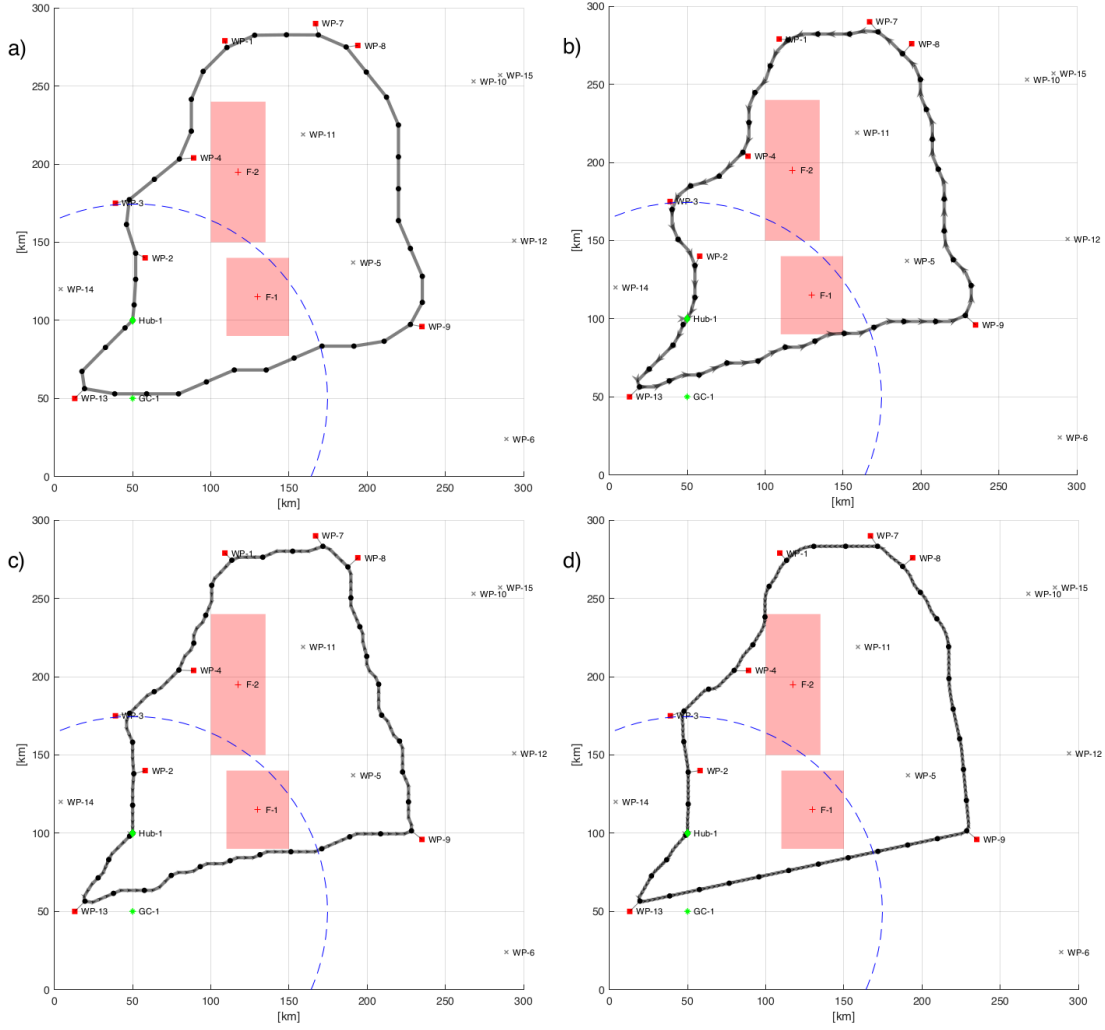





Figure 7: Optimal flight trajectories without fine time steps (a) and for one (b), three (c), and five (d) of them. Each fine time step is represented by an arrow head, describing the UAVs heading.

Table 9: Area and wind velocity per the coordinate direction of the considered wind zones in section 4.2.1.

Wind zone	Area (in km)	Velocity (in $\frac{\text{km}}{\text{h}}$)	Direction
Wind zone 1 (red)	$\begin{pmatrix} 0 \\ 0 \\ 7 \end{pmatrix} - \begin{pmatrix} 300 \\ 300 \\ 20 \end{pmatrix}$	300	
Wind zone 2 (green)	$\begin{pmatrix} 149 \\ 0 \\ 0 \end{pmatrix} - \begin{pmatrix} 300 \\ 300 \\ 8 \end{pmatrix}$	100	
Wind zone 3 (blue)	$\begin{pmatrix} 0 \\ 0 \\ 0 \end{pmatrix} - \begin{pmatrix} 150 \\ 300 \\ 8 \end{pmatrix}$	100	

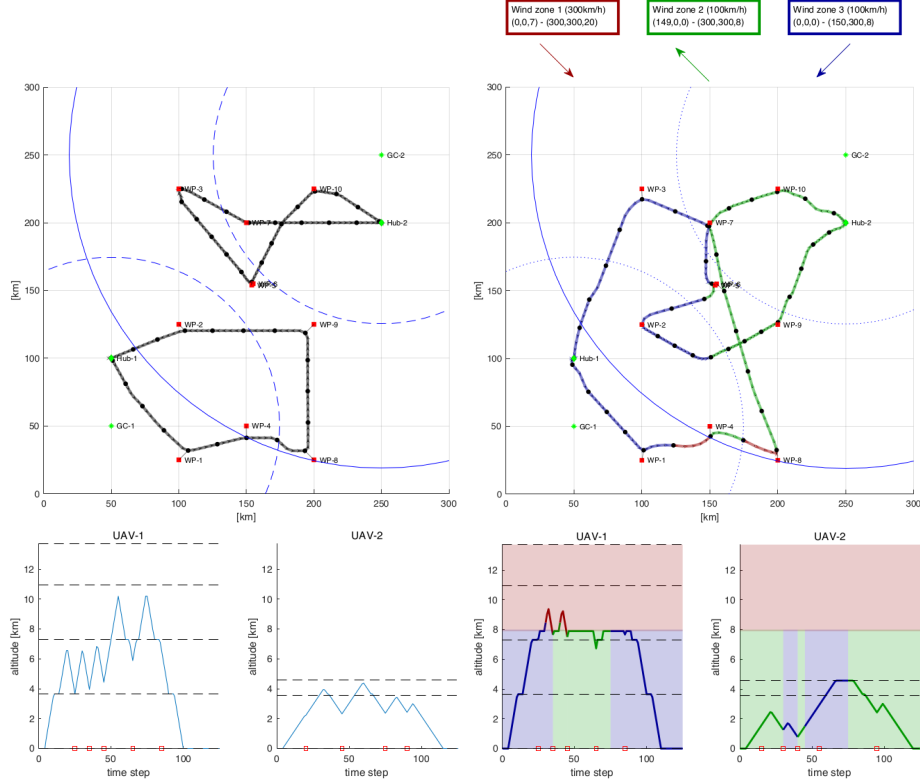


Figure 8: Optimal flight trajectories for the considered instance in absence (*left*) and presence (*right*) of wind. In the presence of wind, the different wind zones are displayed in different colors.

and the obtained altitudes of the UAVs for both cases of the considered instance are given in figure 8. One can see that, in the presence of wind, the assignment from waypoints to UAVs changes. UAV-1 benefits from all three wind zones. At first, it uses wind zone 1 to travel a longer way to waypoint 8, while the time step for visiting it is the same. Then, it stays below wind zone 1 and uses wind zone 2 to visit the more distanced waypoint 3 at the same time step it visits waypoint 9 in the absence of wind. Finally, wind zone 3 is advantageous on the way to the end location. UAV-2 also profits from the wind zones on the way to its first visited waypoint and when it flies to waypoint 2. In the presence of wind, the objective value decreases since both UAVs are longer in midair and UAV-1 has to reduce its altitude to avoid wind zone 1. Regarding the initial fuel, UAV-1 needs 6.6% less (333.57kg instead of 361.53kg), although its trajectory is 31.7% longer (552.34km instead of 419.41km). This fuel saving is the result of the presence of advantageous wind zones. On the other side, UAV-2 needs 15.1% more initial fuel (35.13kg instead of 30.51kg) for its 13.2% longer trajectory (434.33km instead of 383.84km). Since UAV-2 cannot benefit from tailwinds like UAV-1, it needs more fuel for the also longer trajectory.

4.2.2 Altitude-dependent Range

As shown in figure 4, the altitude-dependent approach (2.3') in section 2.3 results in a significant enlarged operating range compared to the constant approach (2.3) with $\varrho_u = 185\text{km}$.

To illustrate the new approach and its limits, we consider both UAVs, two waypoints, 200 time steps without any fine steps each, and $\Delta t = 0.025\text{h}$. The UAVs are stationed at the location of their respective ground control, which is also their start and end location. Furthermore, we set $\varphi_u^{alt,2} = 0.1$, $u \in \mathcal{U}$, to have a better resolution of the increasing

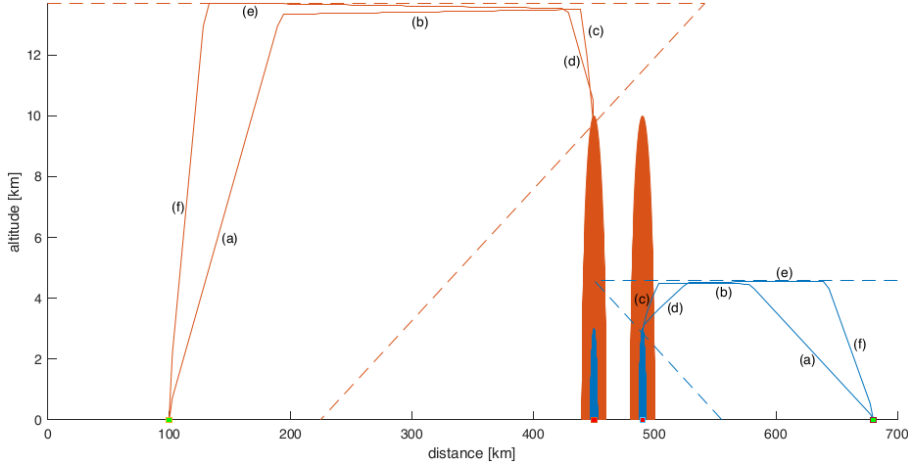


Figure 9: Optimal flight trajectories for the altitude-dependent operating range approach for UAV-1 (*orange*) and UAV-2 (*blue*). Waypoints and ground controls are indicated by a red or green square, respectively. The dashed lines mark the altitude-dependent operating range of the respective UAV and the colored area its maximum operational distance to the waypoints.

maximum flight altitudes of the UAVs. All components of this instance are lined up along the x -axis and both waypoints can be visited at any time step. It took 9,185 seconds to solve this instance to proven global optimality. The optimal flight trajectories of the UAVs are displayed in figure 9.

As shown in figure 9, UAV-1 could reach the position of both points but it cannot visit WP-2 since for the necessary range it requires a flight altitude greater than the maximum operational distance to WP-2. So for visiting all points, UAV-2 has to be deployed, although UAV-1 is near the waypoint. Furthermore, the optimal trajectories can be divided into several phases, marked in figure 9: **(a)** First, both UAVs ascend after takeoff with their maximal ascend rate to reach their mass-dependent maximal altitude. **(b)** Due to the mass reduction by fuel consumption, the maximum altitude of every UAV increases over time so the UAVs keep ascending slowly. This behavior is controlled by the parameters $F_u^{alt,1}$ and $F_u^{alt,2}$. **(c)** Near the respective waypoint, the UAVs slow down and descent to get into the operational range of the waypoint. **(d)** At their point of return, the UAVs achieve the maximum operational distance of the respective waypoint, visit it and start to fly back to their end location since no UAV can get into the operational distance to both points without leaving its operating range. To save fuel, they ascend again to their maximum altitude. **(e)** On their way back, the UAVs can reach a higher altitude compared to the beginning since they consumed most of their initial amount of fuel. **(f)** Every UAV descends to its end location with maximum descent rate to stay in the higher altitude bands as long as possible and benefits from its lower fuel consumption. This approach, to reach the top of descent point before going down, is the most economic descent strategy [23].

4.2.3 Mass-dependent Flight Trajectories

To illustrate the effect of mass-dependent flight dynamics to the computed trajectories, we consider an instance with 10 waypoints, two UAVs, 25 time steps with 4 fine time steps each, and two restricted airspaces and solve it in the presence and absence of mass-dependent flight dynamics. In terms of mass-dependent fuel consumption, we assume the additional fuel per mass factor $\varphi_u^{fuel} = 0.01$ for each UAV $u \in \mathcal{U}$. For the absence of mass dependencies the values $\varphi_u^{fuel} = 0$, $\varphi_u^{acc} = 0$, and $\varphi_u^{alt,2} = 1$ are chosen, while the

parameter $\varphi_u^{alt,1}$ can take an arbitrary value since it is not restrictive. The total amount of CPU time to solve the instance neglecting the mass dependencies was 1044 seconds, while in its presence 3495 seconds were necessary. Figure 10 displays the optimal flight trajectories, altitude and velocity profiles, and the fuel consumption for both instances. As the results in figure 10 indicates, the optimal solution changes in the presence of mass-dependent flight dynamics. Both UAVs have shorter trajectories and return to their end location earlier, while only 8 of 10 waypoints were visited, two less than in the absence of mass dependencies.

While, without the influence of mass, both UAVs use their fastest throttle band and attain their respective maximum velocity, in the presence of the reduction factor φ_u^{acc} , they cannot reach it and must stay in the second-fastest throttle band. Thus, UAV-2 cannot reach waypoint 3 within the given time and, due to the narrow time windows of waypoint 9, none of the UAVs can incorporate this waypoint into its trajectory.

The resulting shorter trajectories are beneficial to the attained altitude of UAV-1. It can now ascend higher since it visits fewer waypoints. But it cannot reach its maximum altitude due to the mass-dependent maximum altitude. For UAV-2, one can see the influence of the abovementioned restriction on its flight dynamics. Whenever it ascends after visiting a waypoint, it can reach a higher altitude since its fuel mass reduces over time.

In terms of the initial amount of fuel, although UAV-1 has a 24.6% shorter trajectory (391.05km instead of 518.87km), it requires 7.0% more initial fuel (from 366.12kg to 391.75kg). In contrast, UAV-2 has an 9.0% smaller amount of initial fuel (from 38.90kg to 35.38kg) for a 36.1% shorter trajectory (286.29km instead of 447.79km). This contrary behavior of UAV-1 is justified in the fuel per mass factor φ_u^{fuel} since it applies as a percentage of the fuel mass. Thus, larger UAVs with higher fuel consumption are affected more than smaller ones and in comparison, UAV-1 can hold nearly four times the amount of fuel of UAV-2.

4.3 Collision Avoidance

In this section, we take a closer look at the computation time of RCPs for an increasing number of UAVs and the quality of the upper bound derived in proposition 3.1. For the following computations, the models described in section 3 were used.

For the two-dimensional case, we consider a circle with center $\vec{C} = (140, 140)$ and radius $r^{RCP} = 90\text{km}$ and use UAVs from the type UAV-1. The safety distances in each coordinate direction are $\varepsilon^i = 9.26\text{km}$, $i \in \{x, y\}$. They are chosen accordingly to the minima for radar separation, published by the International Civil Aviation Organization (ICAO) [13]. For $\Delta t = 0.02$, we get $\underline{T}^{min} = \lceil \frac{180}{232 \cdot 0.02} \rceil = 39$, but we initialize the calculation with $T = 40$ since the initial maximum velocity is reduced by the present mass dependencies.

Varying the number of participating UAVs between 2 and 12, we generate 41 instances and solve them with the described sequential method with a time limit of 3600 seconds for every iteration. The results are displayed in figure 11. For small problems with up to four UAVs, at least 90% of all instances were solved to proven global optimality. In medium-scaled problems with five to nine participating UAVs, this percentage decreases from 61% to 29%, while it drops below 5% for large problems considering ten or more UAVs.

To illustrate the result of proposition 3.1, we generate the upper bound for the necessary number of time steps for the 257 solved instances and compare its minimum and median value against the computed solutions for every number of participating UAVs. In figure 12, one can see that already for small instances with four UAVs, there is a significant gap between the given upper bound and the found optimal solution in both median and minimum value. Furthermore, this gap increases rapidly for larger numbers of UAVs.

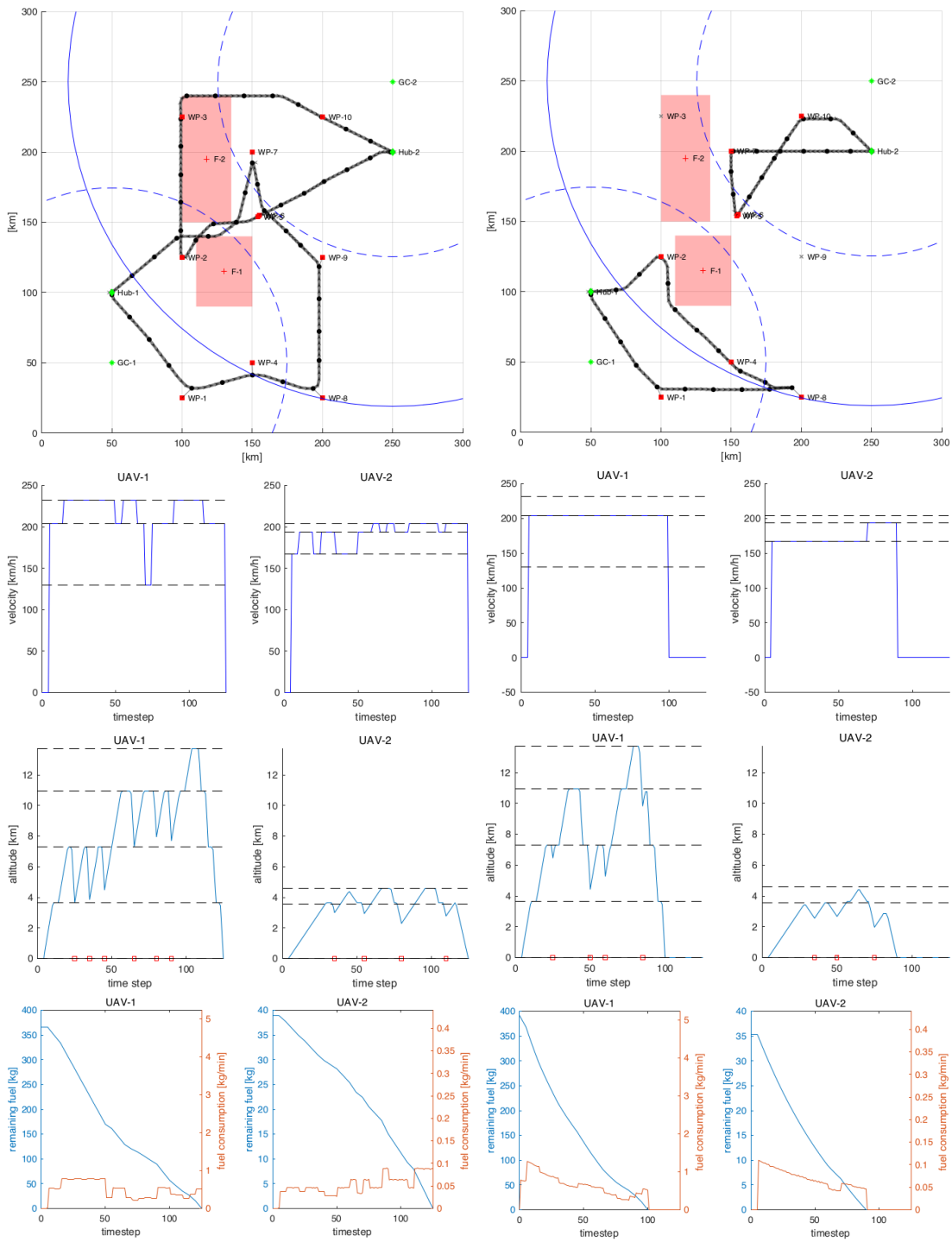


Figure 10: Optimal flight trajectories, altitude and velocity profiles, and the fuel consumption for both UAVs in the absence (*left*) and presence (*right*) of mass-dependent flight dynamics.

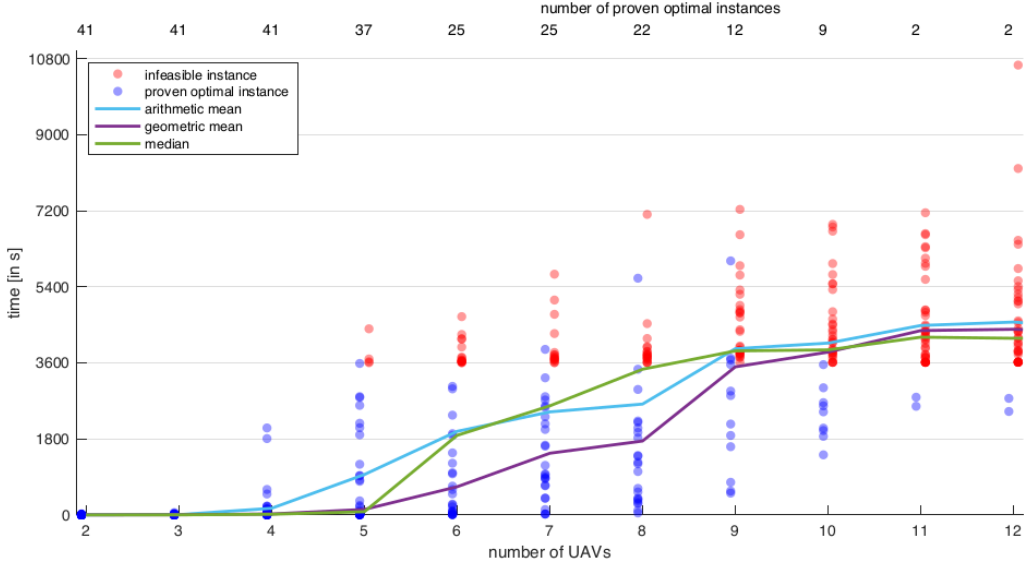


Figure 11: Solution time of the RCP depending on the number of participating UAVs. The count of solved instances for every number of UAVs is displayed above its respective column.

In figure 13, the optimal trajectories of a RCP instance with 14 UAVs are displayed for two different time steps, also including the circle used to calculate the upper bound in proposition 3.1. UAVs 2 and 11 are the first pair violating the given safety distances. Since they start near to each other, the generated circle for the upper bound has radius $r^{ub} = 86.12\text{km}$, which is only about 4% smaller than the original radius r^{RCP} . For the three-dimensional RCP, we take the same parameters as in the two-dimensional case, together with the initial altitude $r_u^z(0) = 10\text{km}$, vertical safety distance $\bar{\varepsilon}^z = 1\text{km}$, and altitude bounds $\underline{h} = 9\text{km}$ and $\bar{h} = 10.972\text{km}$ for all UAVs. Thus, they are all within their second-highest altitude band. The number of participating UAVs is varied between 2 and 20, generating 41 instances for each case. For every computation, there is a time limit of 3600 seconds. Again the described sequential method is used to solve all instances. The results are displayed in figure 14. Allowing the UAVs to avoid conflicts by choosing different altitudes, the solution process is accelerated significantly. Now 676 problems were solved to proven global optimality, while for instances up to 16 participating UAVs, 90% of all cases were solved. Considering at most 13 UAVs, the optimal solution was found within 240 seconds for all problems. For large-scale problems with at least 17 participating UAVs, the number of proven optimal instances rapidly decreases to 10% at the maximum amount of 20 UAVs.

5 Conclusions and Future Work

We extended the mission and flight planning model of [9] by more detailed and mass-dependent flight dynamics, convex shaped restricted airspaces, and wind zones. Two different time discretizations were applied to smooth the resulting trajectories. By linearization, the model got applicable to the MILP solver GUORBI and in numerical tests on a standard computer, several of its aspects were examined. It turned out that the presented model expansions have a significant impact on the computation time by GUORBI. For the class of RCPs, upper bounds for the necessary amount of time steps were derived and compared to the computed optimal solutions.

Our future work will focus on the acceleration of the solution process to solve also

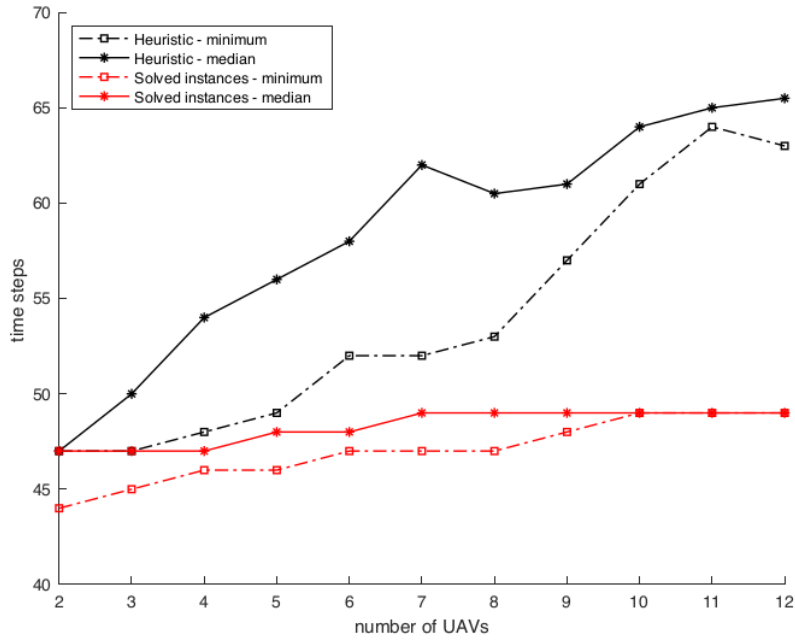


Figure 12: Minimum and the median value of the time steps for the upper bound of proposition 3.1 and the computed optimal solution of all solved instances.

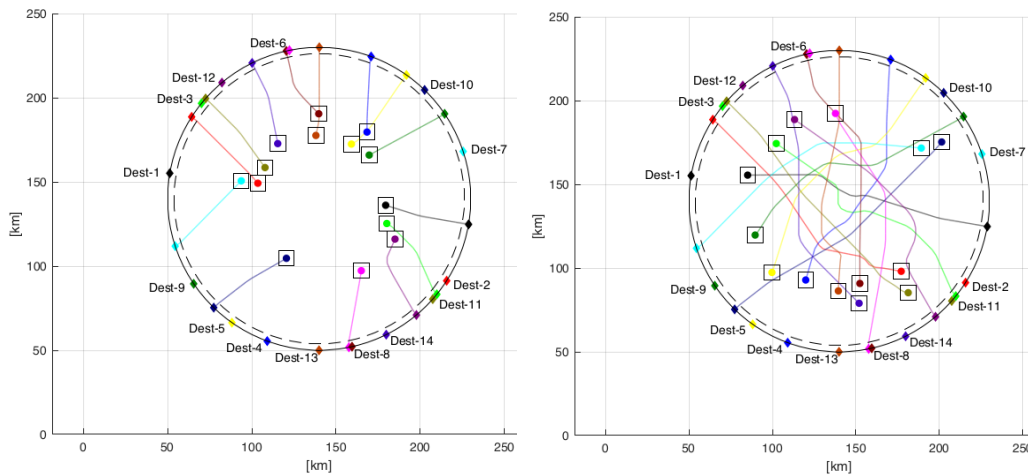


Figure 13: Trajectories of a two-dimensional RCP with 14 UAVs at time steps $t = 13$ (left) and $t = 39$ (right). Start and end location of every UAV are marked by diamonds and the end location is labeled with the number of the UAV. The solid circle displays the underlying circle of the RCP, while the dashed one is part of the computed upper bound.

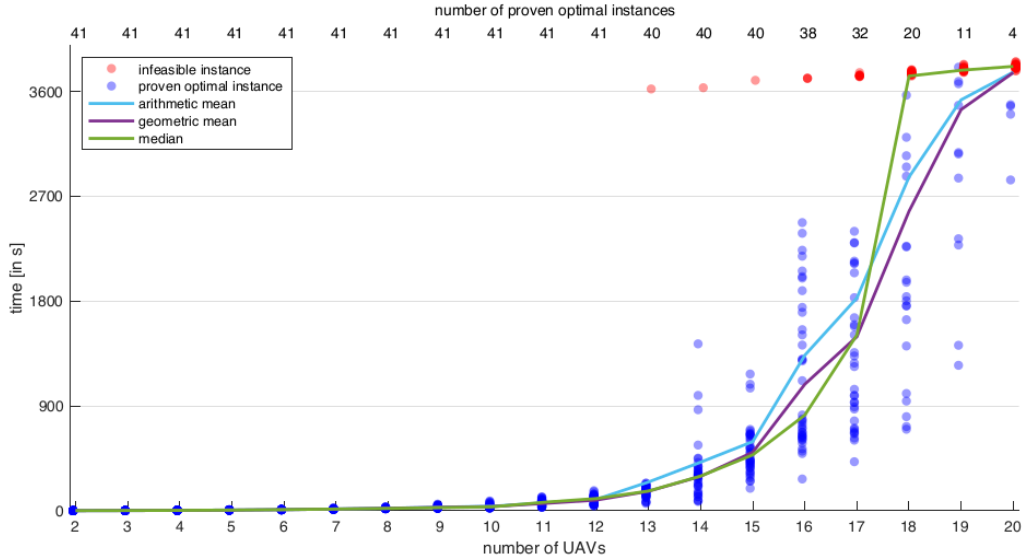


Figure 14: Solution time of the three-dimensional RCP depending on the number of participating UAVs. The count of solved instances for every number of UAVs is displayed above its respective column.

larger instances within a reasonable time and the further extension of the model to more applications.

The authors declare that they have no known competing financial interests or personal relationships that could have appeared to influence the work reported in this paper.

References

- [1] Anders Albert, Frederik S. Leira, and Lars Imsland. UAV Path Planning using MILP with Experiments. *Modeling, Identification and Control*, 38(1):21–32, 2017.
- [2] Peter Auer, György Dósa, Tibor Dulai, Armin Fügenschuh, Peggy Näser, Roland Ortner, and Ágnes Werner-Stark. A new heuristic and an exact approach for a production planning problem. *Central European Journal of Operations Research*, pages 1–35, 2020.
- [3] Yong-bo Chen, Guan-chen Luo, Yue-song Mei, Jian-qiao Yu, and Xiao-long Su. UAV path planning using artificial potential field method updated by optimal control theory. *International Journal of Systems Science*, 47(6):1407–1420, 2016.
- [4] Chun Cheng, Yossiri Adulyasak, and Louis-Martin Rousseau. Drone routing with energy function: Formulation and exact algorithm. *Transportation Research Part B: Methodological*, 139:364–387, 2020.
- [5] Kendra L. B. Cook. The silent force multiplier: The history and role of UAVs in warfare. In *2007 IEEE Aerospace Conference*, pages 1–7, 2007.
- [6] Walton Pereira Coutinho, Jörg Fliege, and Maria Battarra. Glider Routing and Trajectory Optimisation in disaster assessment. *European Journal of Operational Research*, 274(3):1138–1154, 2019.

- [7] Fernando H.C. Dias, Stephanie Rahme, and David Rey. A two-stage algorithm for aircraft conflict resolution with trajectory recovery. *arXiv preprint arXiv:2002.06731*, 2020.
- [8] Dimitris Dranidis. Command: Modern Air/Naval Operations 1.14.7, Database Build 476. Matrix Games, May 30, 2020.
- [9] Armin Fügenschuh, Daniel Müllenstedt, and Johannes Schmidt. Mission planning for unmanned aerial vehicles. *Cottbus Mathematical Preprints*, COMP 6, 2019, 2019. Accepted for publication in MOR.
- [10] Katharina Glock and Anne Meyer. Mission planning for emergency rapid mapping with drones. *Transportation science*, 54(2):534–560, 2020.
- [11] LLC Gurobi Optimization. Gurobi Optimizer Reference Manual, 2020.
- [12] Benno Hoch, Frauke Liers, Sarah Neumann, and Francisco Javier Zaragoza Martínez. The Non-Stop Disjoint Trajectories Problem. http://www.optimization-online.org/DB_FILE/2020/09/8015.pdf, 2020. (Preprint).
- [13] DOC ICAO. 4444 ATM/501. *Procedures for Air Navigation Services–Air Traffic Management (PANS-ATM)*,” *International Civil Aviation Organization, Montreal, Canada*, 2001.
- [14] Fan Kai, Han Songchen, Liao Wenjing, and Liang Binbin. 4D Trajectory Planning of Unmanned Aerial Vehicle in Trajectory Based Operation Airspace. In *Proceedings of the 2019 2nd International Conference on Robot Systems and Applications*, pages 51–58, 2019.
- [15] James K. Kuchar and Ann C. Drumm. The Traffic Alert and Collision Avoidance System. *Lincoln laboratory journal*, 16(2):277–296, 2007.
- [16] Stephen Leary, Markus Deittert, and John Bookless. Constrained UAV mission planning: A comparison of approaches. In *2011 IEEE international conference on computer vision workshops (ICCV workshops)*, pages 2002–2009. IEEE, 2011.
- [17] Bo Li, Xiaogang Qi, Baoguo Yu, and Lifang Liu. Trajectory planning for UAV based on improved ACO algorithm. *IEEE Access*, 8:2995–3006, 2020.
- [18] Vincent Mouillet. User manual for the Base of Aircraft Data (BADA) Revision 3.15. *Eurocontrol Experimental Centre, Cedex, France*, 2019.
- [19] Alena Otto, Niels Agatz, James Campbell, Bruce Golden, and Erwin Pesch. (optimization approaches for civil applications of unmanned aerial vehicles (uavs) or aerial drones: A survey). *Networks*, 72(4):411–458, 2018.
- [20] Cristian Ramirez-Atencia, Gema Bello-Orgaz, María D. R-Moreno, and David Camacho. Solving complex multi-UAV mission planning problems using multi-objective genetic algorithms. *Soft Computing*, 21(17):4883–4900, 2017.
- [21] Marta Ribeiro, Joost Ellerbroek, and Jacco Hoekstra. Review of conflict resolution methods for manned and unmanned aviation. *Aerospace*, 7(6):79, 2020.
- [22] Roberto G. Ribeiro, José R. C. Júnior, Luciano P. Cota, Thiago A. M. Euzébio, and Frederico G. Guimarães. Unmanned Aerial Vehicle Location Routing Problem With Charging Stations for Belt Conveyor Inspection System in the Mining Industry. *IEEE Transactions on Intelligent Transportation Systems*, pages 1–10, 2019.

- [23] Joachim Scheiderer. *Angewandte Flugleistung: eine Einführung in die operationelle Flugleistung vom Start bis zur Landung*. Springer Science & Business Media, 2008.
- [24] Seyed Mahdi Shavarani, Mazyar Ghadiri Nejad, Farhood Rismanchian, and Gokhan Izbirak. Application of hierarchical facility location problem for optimization of a drone delivery system: a case study of Amazon prime air in the city of San Francisco. *The International Journal of Advanced Manufacturing Technology*, 95(9-12):3141–3153, 2018.
- [25] Amila Thibbotuwawa, Grzegorz Bocewicz, Grzegorz Radzki, Peter Nielsen, and Zbigniew Banaszak. UAV Mission Planning Resistant to Weather Uncertainty. *Sensors*, 20(2):515, 2020.
- [26] Marina Torres, David A. Pelta, José L. Verdegay, and Juan C. Torres. Coverage path planning with unmanned aerial vehicles for 3D terrain reconstruction. *Expert Systems with Applications*, 55:441–451, 2016.
- [27] Paolo Toth and Daniele Vigo. *The vehicle routing problem*. SIAM, 2002.
- [28] Jun Xia, Kai Wang, and Shuaian Wang. Drone scheduling to monitor vessels in emission control areas. *Transportation Research Part B: Methodological*, 119:174–196, 2019.
- [29] Ziyang Zhen, Dongjing Xing, and Chen Gao. Cooperative search-attack mission planning for multi-UAV based on intelligent self-organized algorithm. *Aerospace Science and Technology*, 76:402–411, 2018.

IMPRESSUM

Brandenburgische Technische Universität Cottbus-Senftenberg
Fakultät 1 | MINT - Mathematik, Informatik, Physik, Elektro- und Informationstechnik
Institut für Mathematik
Platz der Deutschen Einheit 1
D-03046 Cottbus

Professur für Ingenieurmathematik und Numerik der Optimierung
Professor Dr. rer. nat. Armin Fügenschuh

E fuegenschuh@b-tu.de
T +49 (0)355 69 3127
F +49 (0)355 69 2307

Cottbus Mathematical Preprints (COMP), ISSN (Print) 2627-4019
Cottbus Mathematical Preprints (COMP), ISSN (Online) 2627-6100

www.b-tu.de/cottbus-mathematical-preprints
cottbus-mathematical-preprints@b-tu.de
doi.org/10.26127/btuopen-5461